medRxiv preprint doi: https://doi.org/10.1101/2021.06.29.21259605; this version posted July 3, 2021. The copyright holder for this preprint (which was not certified by peer review) is the author/funder, who has granted medRxiv a license to display the preprint in perpetuity. It is made available under a CC-BY-NC-ND 4.0 International license .

The SARS-CoV-2 receptor-binding domain expressed in Pichia pastoris as a candidate vaccine antigen

Miladys Limonta-Fernández [a,&], Glay Chinea-Santiago [a,&], Alejandro Miguel Martín-Dunn [a,&], Diamile Gonzalez-Roche [a,&], Monica Bequet-Romero [a,&], Gabriel Marquez-Perera [a,&], Isabel González-Moya [a], Camila Canaan-Haden-Ayala [a], Ania Cabrales-Rico [a], Luis Ariel Espinosa-Rodríguez [a],Yassel Ramos-Gómez [a], Ivan Andujar-Martínez [a], Luis Javier González-López [a], Mariela Perez de la Iglesia [a], Jesus Zamora-Sanchez [a], Otto Cruz-Sui [b], Gilda Lemos-Pérez [a], Gleysin Cabrera-Herrera [a], Jorge Valdes-Hernández [a], Eduardo Martinez-Diaz [c], Eulogio Pimentel-Vazquez [c], Marta Ayala-Avila [a], Gerardo Guillén-Nieto [a,d,&,*]

[a] Center for Genetic Engineering and Biotechnology, CIGB, Ave. 31 E/ 158 y 190, La Habana 10600, Cuba.

[b] Civilian Defense Scientific Research Center, Carretera de Jamaica y Autopista Nacional, San José de las Lajas, Mayabeque, Cuba

[c] Biotechnology and Pharmaceutical Industries Group, BioCubaFarma, Ave. Independencia 8126, esq. a Calle 100. Boyeros. La Habana, Cuba.

[d] Latin American School of Medicine, Calle Panamericana Km 3 1/2, Playa, La Habana 11600, Cuba.

[&] These authors contributed equally to this work and should be considered as co-first authors

NOTE: This preprint reports new research that has not been certified by peer review and should not be used to guide clinical practice.

medRxiv preprint doi: https://doi.org/10.1101/2021.06.29.21259605; this version posted July 3, 2021. The copyright holder for this preprint (which was not certified by peer review) is the author/funder, who has granted medRxiv a license to display the preprint in perpetuity. It is made available under a CC-BY-NC-ND 4.0 International license .

* **Corresponding author**:

Gerardo Guillén-Nieto Ph.D.

Biomedical Research Direction

Center for Genetic Engineering and Biotechnology

Ave. 31 E/ 158 y 190, La Habana 10600, Cuba

E-mail: gerardo.guillen@cigb.edu.cu

Abbreviations: Receptor-binding domain (RBD), coronavirus disease 2019 (COVID-19), severe acute respiratory syndrome coronavirus 2 (SARS-CoV-2), angiotensin-converting enzyme 2 (ACE2), peripheral blood mononuclear cells (PBMC), Interleukin 2 (IL-2), Interleukin 4 (IL-4), Interleukin 6 (IL-6), tumor necrosis factor-alpha (TNFα), interferon gamma (IFNγ), non-human primates (NHP), Chinese hamster ovary cells (CHO), baby hamster kidney cells (BHK21), human embryonic kidney cells (HEK293T), immobilized metal ion affinity chromatography (IMAC), reversed-phase chromatography (RP), circular dichroism (CD), optical density (OD), viral neutralization titer (VNT).

Highlights

- The RBD protein (C-RBD-H6 PP) is expressed with high purity in *P. pastoris*.
- Physico-chemical characterization confirms the right folding of the protein.
- The recombinant protein shows high antigenicity with sera from convalescents.
- The sera from animals inhibit the RBD-ACE2 binding and neutralize the virus.

medRxiv preprint doi: https://doi.org/10.1101/2021.06.29.21259605; this version posted July 3, 2021. The copyright holder for this preprint (which was not certified by peer review) is the author/funder, who has granted medRxiv a license to display the preprint in perpetuity. It is made available under a CC-BY-NC-ND 4.0 International license .

- The C-RBD-H6 protein stimulates IFNγ, IL-2, IL-6, IL-4, and TNFα in mice.

1. Abstract

The effort to develop vaccines based on economically accessible technological platforms available by developing countries vaccine manufacturers is essential to extend the immunization to the whole world population and to achieve the desired herd immunity, necessary to end the COVID-19 pandemic. Here we report on the development of a SARS-CoV-2 receptor-binding domain (RBD) protein, expressed in yeast *Pichia pastoris.* The RBD was modified with addition of flexible N- and C-terminal amino acid extensions aimed to modulate the protein/protein interactions and facilitate protein purification. Fermentation with yeast extract culture medium yielded 30–40 mg/L. After purification by immobilized metal ion affinity chromatography and hydrophobic interaction chromatography, the RBD protein was characterized by mass-spectrometry, circular dichroism, and binding affinity to angiotensin-converting enzyme 2 (ACE2) receptor. The recombinant protein shows high antigenicity with convalescent human sera and also with sera from individuals vaccinated with the Pfizer-BioNTech mRNA or Sputnik V adenoviral-based vaccines. The RBD protein stimulates IFNγ, IL-2, IL-6, IL-4, and TNFα in mice secreting splenocytes from PBMC and lung CD3+ enriched cells. Immunogenicity studies with 50 µg of the recombinant RBD formulated with alum, induce high levels of binding antibodies in mice and non-human primates, assessed by ELISA plates covered with RBD protein expressed in HEK293T cells. The mouse sera inhibited the RBD binding to ACE2 receptor in an *in-vitro* test and show neutralization of SARS-CoV-2 infection of Vero E6 cells. These data suggest that the RBD recombinant

medRxiv preprint doi: https://doi.org/10.1101/2021.06.29.21259605; this version posted July 3, 2021. The copyright holder for this preprint (which was not certified by peer review) is the author/funder, who has granted medRxiv a license to display the preprint in perpetuity. It is made available under a CC-BY-NC-ND 4.0 International license .

protein expressed in yeast *P. pastoris* is suitable as a vaccine candidate against COVID-19.

Keywords: SARS-CoV-2, *P. pastoris*, COVID-19, RBD, subunit vaccine

1. Introduction

The pandemic caused by SARS-CoV-2 has demonstrated the need to modify the way that public health, the governmental role, and international cooperation in science and health have been functioning up to now. It will not be possible to end the pandemic if the desired herd immunity is not achieved and for that it is necessary to vaccinate the vast majority of the world's population in the shortest possible time. It is not enough for industrialized countries to be vaccinated, so the contribution of the developing countries' vaccine manufacturers is more than welcome.

Cuba is an example of a global vision of public health and stands out for the strength of its biotechnology industry where one of the main achievements is the production of the Hepatitis B recombinant vaccine in yeast *P. pastoris* since 1991 [1-3] and the inclusion in the national immunization program since 1992. As a result, the incidence of acute hepatitis B in the country has decreased down to less than 50 cases and acute hepatitis B in children under 5 years old has not been reported since the year 2000 [4].

Therefore, it is feasible to select this technological platform for the development of a vaccine candidate against SARS-CoV-2.

The mammalian cell expression systems as Chinese hamster ovary cells (CHO), baby hamster kidney cells (BHK21), human embryonic kidney cells (HEK293T), and mouse-

medRxiv preprint doi: https://doi.org/10.1101/2021.06.29.21259605; this version posted July 3, 2021. The copyright holder for this preprint
(which was not certified by peer review) is the author/funder, who has granted medRxiv a license to display the preprint in perpetuity.
It is made available under a CC-BY-NC-ND 4.0 International license .

derived myeloma cell lines (NS0, SP2/0) are preferred for the expression of complex proteins for its capacity of proper post-translational modifications equivalent to that of humans, even though the selection of this recombinant protein production platform is limited by its low growth and productivity, and high production cost due to the relevant nutrient requirement [5]. The potential viral contamination of culture medium has also limited the use of the mammalian cell expression systems in large-scale production [6].

Pichia pastoris is one of the biotechnological platforms for the production of recombinant proteins that overcome several limitations of bacteria as expression system, such as protein aggregation and misfolding, production of toxic lipopolysaccharides, lack of posttranslational modifications, and frequent protein degradation due to the presence of proteases [7]. N-glycans in yeast secreted proteins are highly mannosylated while mammalian proteins have hybrid sugar composition. *P. pastoris* uses methanol, an inductor of the strong and tightly regulated AOX1 promoter as an exclusive carbon source. Therefore methanol can be used to drive protein expression altogether that it is reached an efficient secretion of the recombinant proteins [8]. On the other hand, the advantages of protein production by *P. pastoris* lie in the fact that the mechanism of protein expression in these microorganisms is close to the ones in mammalian cells and include the right protein folding in the endoplasmic reticulum, protein secretion by Kex2 as signal peptidase and low contamination with host proteins due to its limited production of endogenous secretory proteins [9], which simplifies and makes the purification process more feasible. Other significant advantages of yeast include growth speed, and easy genetic manipulation allowing

medRxiv preprint doi: https://doi.org/10.1101/2021.06.29.21259605; this version posted July 3, 2021. The copyright holder for this preprint
(which was not certified by peer review) is the author/funder, who has granted medRxiv a license to display the preprint in perpetuity.
It is made available under a CC-BY-NC-ND 4.0 International license .

linearized foreign DNA to be inserted at high efficiency in a chromosome via cross recombination to generate stable cell lines [10].

The receptor-binding domain of SARS-CoV-2 is a glycosylated 25 kDa protein domain spanning residues N_{331}-K_{529} of the spike protein, including eight cysteine residues forming four disulfide bonds. The domain contains two glycosylation sites (N_{331} and N_{343}) and a central twisted antiparallel beta-sheet formed by five strands with secondary structure short helices and loops [11]. Although glycosylation plays a fundamental role in the immunogenicity and stability of the RBD protein, the variability of the composition and heterogeneity in size of the sugar chains may not influence the receptor binding capacity [12]. Probably, for this reason the glycosylation introduced by *P. pastoris* more distant from mammalian cells and therefore more distant to the humans could contribute to the protein immunogenicity. RBD mediates cell entry through ACE2 host receptor and the levels of RBD binding antibodies strongly correlate with neutralizing antibodies in patients. Even more, the neutralizing antibody kinetics in patients mirrored the kinetics of RBD antibody development [13]. Since RBD upon infection is the main target of neutralizing antibodies, it has become the focus of vaccine design.

The SARS-CoV-2 RBD has been expressed at high levels in *P. pastoris* as a suitable vaccine candidate against COVID-19 [8;14;15]. The comparison between RBD obtained from *P. pastoris* and HEK293T mammalian cells by CD and tryptophan fluorescence shows that proteins were properly folded as well as that they have similar temperature stability despite differences in glycosylation of both expression platforms.

Here, we report the design of an RBD protein vaccine candidate, its expression in *P. pastoris* yeast, protein purification, the physico-chemical characterization and the

medRxiv preprint doi: https://doi.org/10.1101/2021.06.29.21259605; this version posted July 3, 2021. The copyright holder for this preprint
(which was not certified by peer review) is the author/funder, who has granted medRxiv a license to display the preprint in perpetuity.
It is made available under a CC-BY-NC-ND 4.0 International license .

capacity of the protein to elicit ACE2 binding inhibition antibodies, and neutralizing response in mice and monkeys. Our approach differs from the previously reported expression of RBD in *P. pastoris* [8] in the inclusion of the RBD glycosylation sites maintaining the advantage of the glycosylation capacity of *P. pastoris*.

2. Materials and Methods

2.1. Biological reagents, protein codification and serum panels

Human and murine RBD and ACE2 receptor chimeric proteins (hFc-RBD, mFc-RBD, hFc-ACE2, mFc-ACE2) were supplied by the Center of Molecular Immunology (CIM, Havana, Cuba). All the chimeric proteins were purified by protein-A based purification of the supernatant of stable transduce HEK293T cells and eluted in PBS. hFc-RBD was conjugated with peroxidase (HRP) and henceforth named hFcRBD-HRP. H6-RBD was produced as *E. coli* inclusion bodies [16], while RBD-H6 and C-RBD-H6 HEK were secreted to the supernatant of stably transduced HEK293T. All three proteins were purified by IMAC and the final buffer was exchanged to PBS. N-terminal end segment (C), and C-terminal end six histidine tag (H6), added to the central RBD protein sequence in a different protein constructions are codified as C-RBD-H6. Acronyms PP and HEK next to the protein code refers to the expression system when *P. pastoris* or HEK293T cells where used.

Different human sera used as controls include sera from volunteers vaccinated with Pfizer/BioNtech or Gamaleya's Sputnik V (Gam-COVID-Vac) vaccine, and sera from convalescent patients. All individuals gave their writing informed consent for the use of their serum.

medRxiv preprint doi: https://doi.org/10.1101/2021.06.29.21259605; this version posted July 3, 2021. The copyright holder for this preprint (which was not certified by peer review) is the author/funder, who has granted medRxiv a license to display the preprint in perpetuity. It is made available under a CC-BY-NC-ND 4.0 International license .

2.2. Construction of Pichia pastoris strains expressing RBD from SARS-CoV-2 (C-RBD-H6 PP)

A sequence coding for residues 331-530 of the Spike protein of SARS-CoV-2 strain Wuhan-Hu-1 (NCBI Acc. No. YP_009724390) with the appropriate N- and C-terminal extensions was codon-optimized for *S. cerevisiae* using J-Cat [17] and cloned in-frame with the KEX2 cleavage site of the pre-pro MATα sequence of pPICZαA (Invitrogen, USA), placing it under transcriptional control of the *P. pastoris* AOX1 promoter. After sequence verification, a representative clone was used to transform *P. pastoris* strain X-33 [18], selecting transformants by plating in YPD agar at Zeocin™ concentrations of 100, 200, 400, and 800 µg/mL. Three transformants from the plate with the highest concentration of Zeocin™ were randomly picked, purified by further streaking on YPD-Zeocin™, and used to prepare small seed banks. The seed banks were used in turn to inoculate small-scale (50 mL) BMGY cultures [18] that were induced after 24 h of growth at 28 °C by the addition of 0.5 % methanol. Culture supernatants were analyzed at 96 h post-induction by SDS-PAGE and Western blotting with an anti-His6 antibody (Promega, USA).

2.3. Fermentation

Fermentation was carried out in a 75-liters Chemap fermenter (Germany) with a working volume of 50 L of fermentation medium containing per liter of culture 8.8 mL of 85 % phosphoric acid, 6.92 g $MgSO_4.7H_2O$, 1.23 g $(NH_4)_2SO_4$, 16.77 g K_2HPO_4, 0.46 g $CaCl_2.2H_2O$, 32.3 mL of 98% glycerol, 4.61 g yeast extract, 4 mL histidine solution, 5 mL of 400X vitamin base solution (1 g L^{-1} myo-inositol, 0.8 g L^{-1} D-calcium

medRxiv preprint doi: https://doi.org/10.1101/2021.06.29.21259605; this version posted July 3, 2021. The copyright holder for this preprint (which was not certified by peer review) is the author/funder, who has granted medRxiv a license to display the preprint in perpetuity. It is made available under a CC-BY-NC-ND 4.0 International license .

pantothenate, 0.8 g L^{-1} thiamine hydrochloride, 0.8 g L^{-1} pyridoxol hydrochloride, 0.2 g L^{-1} nicotinic acid, 0.8 mg L^{-1} D (+) Biotin), and 1 mL of sterile-filtered trace 1000X element solution (6 g L^{-1} $CuSO_4.5H_2O$, 0.415 g L^{-1} KI, 3 g L^{-1} $MnSO_4.H_2O$, 1 g L^{-1} $Na_2MoO_4.2H_2O$, 0.1 g L^{-1} H_3BO_3, 20 g L^{-1} $ZnSO_4.7H_2O$, 65 g L^{-1} $FeSO_4.7H_2O$, 10 mL. conc.H_2SO_4) was added after autoclaving [19]. After inoculation of the bioreactor with 4 L of pre-culture, the temperature was maintained at 30 °C and the pH at 4.75 by pumping in a liquid ammonia solution. When a dissolved oxygen peak or a widening of the pH peaks is observed, the fed-batch phase is started with glycerol 50 % at 540 mL/h for 2-3 h. After one hour, the temperature is lowered to 25 ° C and raises the pH to 5.5. When the 50 % glycerol increase is exhausted, 800 mL of methanol is added at maximum flow of the peristaltic pump. The induction phase with methanol is started at an initial flow of 240 mL/h, 4 h later the flow is increased to 380 mL/h, and then at 480 mL/h. This last flow is maintained until the end of fermentation (38-44 h).

2.4. Protein purification

After 48 h of fermentation in a yeast extract culture medium, the culture was harvested, and cells were removed by centrifugation retention time between 5 -10 min at 15000 rpm at 4 ^{o}C. The fermentation supernatant was filtered in tandem conditions from 8 µm – 3 µm – 0.45 µm using cellulose filters. The supernatant was concentrated with a tangential flow filtration system with 30 kDa Hydrosart® membrane (Sartorius, Germany), besides buffer exchanged was carried out against PBS buffer containing 5 mM of imidazole. The IMAC column (Chelating Sepharose™ FF, Cytiva) was equilibrated in the same buffer and the sample was loaded and sequentially washed by using 30 column volumes of PBS containing 10 mM and 20 mM imidazole. Elution was

medRxiv preprint doi: https://doi.org/10.1101/2021.06.29.21259605; this version posted July 3, 2021. The copyright holder for this preprint (which was not certified by peer review) is the author/funder, who has granted medRxiv a license to display the preprint in perpetuity. It is made available under a CC-BY-NC-ND 4.0 International license .

carried out by increasing the concentration of imidazole up to 250 mM in the equilibrium buffer. The eluted protein was applied to a RP C4 column (Tosohaas, Japan) with dimensions 50 mm in diameter by 250 mm long for a resin volume of 500 mL and with a particle size of 15 to 20 µm. The column is coupled to a Shimadzu model LC-20AP semi-preparative HPLC purification system. The column was equilibrated with 0.5 % TFA solution, and protein was eluted by using a linear gradient of 1 % TFA solution (RP solution A) and acetonitrile with 0.5 % TFA (RP solution B) from 32 to 45 % solution B in 40 minutes. The protein elutes between 35 and 37 % of solution B, approximately in one column volume. The fraction collected with the purified protein was concentrated by tangential flow filtration system with a 10 kDa Hydrosart® membrane and pooled aseptically using a 0.22 µm and stored at -20 ^{o}C.

2.5. ESI-MS analysis of the deglycosylated C-RBD-H6 PP protein

The volume equivalent to 100 µg of the protein dissolved in PBS (pH 7.2) was deglycosylated with 1µL of PNGase-F (500 units, New England Biolabs) in presence of 0.5 M guanidine hydrochloride and 5 mM N-ethylmaleimide during 2 h at 37 ^{o}C. An aliquot of 10 µg of deglycosylated protein was desalted by using ZipTip C18 (Millipore) and the elution was loaded into the metal-coated nanocapillary for ESI-MS analysis. The remaining deglycosylated protein was digested by using an in-solution buffer-free trypsin digestion protocol previously reported [20] and adapted to the analysis of SARS-CoV-2 RBD proteins by introducing some modifications that provide full-sequence coverage and detection of post-translational modifications in a single ESI-MS spectrum

medRxiv preprint doi: https://doi.org/10.1101/2021.06.29.21259605; this version posted July 3, 2021. The copyright holder for this preprint
(which was not certified by peer review) is the author/funder, who has granted medRxiv a license to display the preprint in perpetuity.
It is made available under a CC-BY-NC-ND 4.0 International license .

[16]. Other experimental conditions for ESI-MS analysis are similar to those reported previously [16].

2.6. Surface plasmon resonance experimental procedure

The interaction between mFc-ACE2 fusion protein and the recombinant C-RBD-H6 PP was monitored by SPR using a BIACORE X (GE Health-care) at 25 °C in a multi-cycle mode. Briefly, mFc-ACE2 was immobilized on a Protein A biosensor chip (GE Health-care) according to the manufacturer's protocol through the flow cell 1 (FC1). The FC2 was used as the reference cell. The real-time response of the C-RBD-H6 PP over the immobilized mFc-ACE2 was recorded by duplicate in a concentration range from 15 to 2000 nM, at 10 µL/min flow rate for 120 s, while the dissociation took place for another 120 s. The running buffer was PBS (pH = 7.2). After each cycle the chip was regenerated using pH = 2.0 glycine buffer. The equilibrium dissociation constant (binding affinity, K_D) was estimated with the BIAevaluation® software (GE Healthcare) using the Langmuir 1:1 interaction model. At least five curves were taken into account for kinetics calculations.

2.7. Structural Analysis by Circular Dichroism (CD) Spectroscopy

CD spectra were acquired in a Jasco J-1500 CD spectrometer (Jasco, Japan). All measurements were carried out at 24 °C, the far UV CD spectra were studied at 100 µg/ml protein concentration (a 10 fold dilution in water of the stock solution) using a 1mm quartz cuvette. The near UV CD spectra were studied at the protein concentration of the stock solution in 20 mM pH 7.4 Tris buffer using a quartz cuvette of 10 mm path length. The spectra of the corresponding solution were subtracted. The far UV CD

medRxiv preprint doi: https://doi.org/10.1101/2021.06.29.21259605; this version posted July 3, 2021. The copyright holder for this preprint
(which was not certified by peer review) is the author/funder, who has granted medRxiv a license to display the preprint in perpetuity.
It is made available under a CC-BY-NC-ND 4.0 International license .

241 spectra were further analyzed by the BeStSel method [21;22] to estimate the secondary
242 structure content of the protein and the results were compared with the values derived
243 from the 3D coordinates of the crystallographic structure of the spike protein of SARS-
244 CoV-2 (PDB file 6yla) using DSSP method [23] implemented in Whatif program package
245 [24].

246 ***2.8. Animals and immunization schedules***

247 Three different animal species were used for evaluation of immunogenicity of the C-
248 RBD-H6 PP protein: BALB/c mice, Sprague–Dawley (SD) rats, and African green
249 monkeys (*Chlorocebus aethiops sabaeus*). Six- to eight-week-old female BALB/c mice,
250 and male and female SD rats were used for the study and housed in the animal facility.
251 The experimental protocols were approved by the Ethical Committee on Animal
252 Experimentation of the Center for Genetic Engineering and Biotechnology (CIGB,
253 Havana, Cuba) and the Center for Production of Laboratory Animals (CENPALAB,
254 Bejucal, Cuba).

255 The immunogen content per 500 µL: 50 µg of C-RBD-H6 PP protein adjuvated with 0.3
256 mg of aluminum hydroxide gel (Alhydrogel ®) in phosphate buffer (0.28 mg of disodium
257 hydrogen phosphate, 0.31 mg of sodium dihydrogen phosphate dihydrate, 4.25 mg of
258 sodium chloride).

259 *BALB/c mice*: Immunogenicity in mice was evaluated using a three-dose schedule with
260 a 50 µg dose by intraperitoneal route with a 7 and 14 days interval before the second
261 and third doses respectively. Blood was collected a week after the first boost and 7 and

medRxiv preprint doi: https://doi.org/10.1101/2021.06.29.21259605; this version posted July 3, 2021. The copyright holder for this preprint
(which was not certified by peer review) is the author/funder, who has granted medRxiv a license to display the preprint in perpetuity.
It is made available under a CC-BY-NC-ND 4.0 International license .

14 days after the second boost. The number of animals per group, age, and gender of the animals are described in individual experiments.

Sprague Dawley rats: Immunogenicity of the C-RBD-H6 PP protein was tested in 20 SD rats (10 male and 10 female) during chronic toxicology study, with a 9 µg dose administered by the intramuscular route once a week, for 10 consecutive weeks for a total of 90 µg. Animals were bled three days after the last dose.

Chlorocebus aethiops sabaeus non-human primates: NHP ages between 3 to 6 years and with 2-7 kg of weight were kept at the animal's facility at the CENPALAB. A total of 20 NHP were randomly assigned to 3 groups including the placebo (2 animals/gender, total 4), the low dose (50 µg, 3 animals/gender, total 6), and the high dose (100 µg, 5 animals/gender, total 10). Seven days post-1st and 2nd boosting and after overnight fasting, monkeys were sedated by intramuscular injection of ketamine hydrochloride (10 mg/kg) and bled from the femoral vein.

Specific anti-RBD titers and the inhibition of its interaction with ACE2 receptor were evaluated using ELISA. Live SARS-CoV-2 neutralization was assessed using a microneutralization assay.

2.9. Serum antibodies evaluation

Antibody detection by ELISA

The reactivity of sera from immunized animals was determined by ELISA. Briefly, 0.25 µg of RBD protein produced in HEK293T cells (Center for Molecular Immunology, Havana) was used to coat 96-well microtiter plates (Corning Costar, Acton, MA) in 0.1 M sodium carbonate buffer (pH 9.6) at 4 °C overnight. After the plates were blocked

medRxiv preprint doi: https://doi.org/10.1101/2021.06.29.21259605; this version posted July 3, 2021. The copyright holder for this preprint
(which was not certified by peer review) is the author/funder, who has granted medRxiv a license to display the preprint in perpetuity.
It is made available under a CC-BY-NC-ND 4.0 International license .

with 2 % skim milk, 0.05 % Tween 20, serially diluted mouse, rat or NHP sera or control monoclonal antibodies SS-1, SS-4, SS-7 and SS-8 (Center for Genetic Engineering and Biotechnology, Sancti Spiritus, Cuba), were added and incubated at 37 °C for 2 h in 0.2 % skim milk, 0.05 % Tween 20 in PBS, followed by six washes with PBS containing 0.05 % Tween 20. Bound antibodies were detected with horseradish peroxidase-conjugated goat anti-mouse IgG (SIGMA, USA), anti-Rat IgG (SIGMA, USA) anti-human IgG (1:10000, Jackson, USA) at 37 °C for 1 h, followed by washes. The reaction was detected after the addition of 3,3-5,5-tetramethylbenzidine and quantified using a microplate reader at 450 nm (BMG Labtech, Germany). This assay was also used for the evaluation of RBD antigenicity using sera from immunized animals, and from subjects that received Pfizer-BioNTech or Sputnik V vaccines, or are COVID-19 convalescents.

RBD to ACE2 plate-based binding assay

A competitive ELISA was performed to determine the inhibitory activity of the anti-RBD polyclonal sera on the binding of the hFc-ACE2 coated plates to an hFc-RBD-HRP conjugate. Briefly, the wells of ELISA plates were coated with 0.25 µg of recombinant hFc-AEC2 as described above. A mixture containing an hFc-RBD-HRP conjugate and serial dilutions of the sera were pre-incubated for 1h at 37 °C. A hundred microliters of the mixture were added to hFc-ACE2 coated plates and further incubated for 90 min at 37 °C. The binding of the HRP tagged RBD to the receptor was detected after the addition of 3,3-5,5-tetramethylbenzidine and reading at 450 nm. A similar assay was used to characterize the ability of the C-RBD-H6 PP and C-RBD-H6 HEK proteins to block the interaction of hFc-RBD-HRP with coated hFc-ACE2.

medRxiv preprint doi: https://doi.org/10.1101/2021.06.29.21259605; this version posted July 3, 2021. The copyright holder for this preprint (which was not certified by peer review) is the author/funder, who has granted medRxiv a license to display the preprint in perpetuity. It is made available under a CC-BY-NC-ND 4.0 International license .

2.10. Microneutralization of live SARS-CoV-2 virus in Vero E6

The neutralization antibody titers were detected by a traditional virus microneutralization assay (MN50) using SARS-CoV-2 (CUT2010-2025/Cuba/2020 strain). Vero E6 cells (2×10^4 per well) were seeded in 96-well plates one night before use. Animals' sera were inactivated at 56 °C for 30 min. The samples were prepared by two-fold serial sera dilutions in the Eagle's Minimal Essential Medium (MEM, Gibco, UK) containing 2 % (v/v) fetal bovine serum (Capricorn, Germany). SARS-CoV-2 strain at 100 TCID50 was incubated in the absence or presence of diluted sera for 1 h at 37 °C. Afterward, Vero E6 cell were overlaid with virus suspensions. At 96 h post-infection, the cells were inspected for signs of cytopathogenic effects (CPE) by optical microscopy and stained with neutral red (Sigma, USA). After three washes neutral red was dissolved in lysis solution (50 % ethanol, 1 % acetic acid) for 15 min at 25 °C, and optical density (OD) was detected at 540 nm. The highest serum dilution showing an OD value greater than the cut-off was considered as the neutralization titer. The cut-off value is calculated as the average of the OD of the cell control wells divided by two. The viral neutralizing titers (VNT50) were calculated as the highest serum dilution at which 50 % of the cells remain intact according to neutral red incorporation in the control wells (no virus added).

2.11. Cellular immune response

Long-term cellular immune response was evaluated in BALB/c mice using subcutaneous administration of a formulation containing an equal antigen to alum ratio. Animals receive 25 µg of the C-RBD-H6 PP antigen by the subcutaneous route in a 100 µL volume in a 0-14-35 days schedule. Blood samples were evaluated two weeks after

medRxiv preprint doi: https://doi.org/10.1101/2021.06.29.21259605; this version posted July 3, 2021. The copyright holder for this preprint
(which was not certified by peer review) is the author/funder, who has granted medRxiv a license to display the preprint in perpetuity.
It is made available under a CC-BY-NC-ND 4.0 International license .

the last immunization and animals were euthanized 3 months later to assess for systemic and lung resident cells response to *in vitro* antigen recall. Splenocytes were flushed out by perfusion using gentamycin supplemented PBS and lung resident lymphocytes were extracted after elimination of remnant blood by left auricular perfusion with PBS. To detach leukocytes from lung tissue, a lung dissociation enzyme mix (130-095-927, Miltenyi, Germany) was used according to manufacturer instructions and using a cell dissociator (GentleMACS Octo Dissociator, Miltenyi). CD3+ cells were further selected from lung suspension using negative selection with magnetic beads (130-095-130, Miltenyi) and both lung CD3+ cells and splenocytes live cells were counted using a flow cytometer (CyFlow, Sysmex, Germany).

For the re-stimulation assays, splenocyte or lung selected CD3+ suspensions were diluted to $10x10^6$ CD3+ live cells/mL and 50 µL of each sample was seeded in two 96-well U bottom tissue culture plates. Cells were re-stimulated with 50 µL of 20 µg/mL C-RBD-H6 PP, or just media (unstimulated) for 72 h, and the supernatant was analyzed at 1:2 dilution using Biolegend Deluxe cytokine kits for IL-2 (431004), IFNγ (430804), IL-6 (431304), IL-4 (431104) and TNFα (430204) following manufacturer's instructions. Cells were transferred at that point to anti IFNγ coated ELISpot plates (Mabtech, Germany) and results were analyzed 24 h later according to established procedures.

2.12. ELISpot assay with samples from previous naturally infected individuals

PBMCs from subjects with previous natural infection with SARS-CoV-2 were isolated from 7 mL of whole blood collected using CPT tubes (Becton Dickinson, US), and store in liquid nitrogen until analyzed. After overnight resting the cells in Optmizer media

medRxiv preprint doi: https://doi.org/10.1101/2021.06.29.21259605; this version posted July 3, 2021. The copyright holder for this preprint (which was not certified by peer review) is the author/funder, who has granted medRxiv a license to display the preprint in perpetuity. It is made available under a CC-BY-NC-ND 4.0 International license .

(Gibco, Invitrogen, US) CD3+ live cells were counted using flow cytometry and seeded on activation plates at $5x10^4$ cells per well with 10 µg/mL of the recombinant C-RBD-H6 PP protein for 72 h. After transferring the cells to anti-IFNγ pre-coated plates (Mabtech, GE). The amounts of T cells secreting the cytokine were detected after 20 h of incubation as recommended by the manufacturer. All individuals gave their writing informed consent for the use of their samples.

2.13. Statistical analysis

Prism 8.4.3 software was used to generate dose-response curves for ELISA test and to calculate EC50 values when needed. One way-ANOVA with Sidak's multiple comparisons tests-was used to determine the significance of differences and Spearman test was used to assess for parameters correlations. Wilcoxon matched paired test was used to perform paired analyzes for both stimulated/non-stimulated samples, the evolution of RBD specific titers and inhibition of ACE2 binding.

3. Results

3.1. Design of the C-RBD-H6 expression cassette

Recombinant C-RBD-H6 PP protein was designed as a potential subunit vaccine candidate against SARS-CoV-2 displaying e modular structure consists of: a) a globular central – RBD- domain comprising residues N_{331}-K_{529} of the spike protein, b) additional N- and C-terminal segments including polar and flexible linkers rich in Glycine and Serine (Gly^9-Ser^{15} and Gly^{215}-Ser^{229}). The N- and C-terminal extensions are aimed to modulate potential protein-protein interactions and facilitate protein purification through

medRxiv preprint doi: https://doi.org/10.1101/2021.06.29.21259605; this version posted July 3, 2021. The copyright holder for this preprint (which was not certified by peer review) is the author/funder, who has granted medRxiv a license to display the preprint in perpetuity. It is made available under a CC-BY-NC-ND 4.0 International license .

a high accessible hexa-Histidine tag (His^{232}-His^{237}). Topologically, the extensions are located in the opposite site of the protein respect to the receptor binding motif and its presence should sterically hinder potential aggregation problems associated to the presence of the exposed and disulfide bonded Cys^{76} and Cys^{210}. (The C-RBD-H6 PP protein sequence is included as a supplemental material S1).

3.2. Expression and purification of the C-RBD-H6 PP

A construct for the expression in *P. pastoris* of the RBD from SARS-CoV-2 under control of the AOX1 promoter, denominated pPICZα-CtagRBDH6, was prepared as described in Materials and Methods and used to obtain RBD-expressing yeast clones. Fig. 1 (lanes A-C) shows the result of the analysis of culture supernatants from 3 randomly selected clones after induction with methanol. There is a noticeable smear in the supernatant from all three clones, ranging between 25 kDa and 50 kDa, that is absent from the control transformed with the empty vector (lane V, Fig. 1), and resolves into a ladder when probed by Western blotting with an anti-His6 antibody. Considering the presence of three-potential N-glycosylation sites in the sequence of C-RBD-H6 PP protein; and also that its molecular mass calculated from its cDNA sequence is 26 kDa the presence of a broad and diffuse band detected on SDS-PAGE analysis suggest that the C-RBD-H6 PP is being secreted in all three cases as a N-glycosylated protein. Based on signal intensity in Western blotting, clone C was denominated X33-23 and selected for further work (Fig. 1). The C-RBD-H6 PP protein was purified from the supernatant following the procedures described in Materials and Methods, by IMAC, followed by polishing using a RP to obtain a final preparation with high purity. After purification, the C-RBD-H6 PP was obtained with a final yield between 30–40 mg/L of

medRxiv preprint doi: https://doi.org/10.1101/2021.06.29.21259605; this version posted July 3, 2021. The copyright holder for this preprint (which was not certified by peer review) is the author/funder, who has granted medRxiv a license to display the preprint in perpetuity. It is made available under a CC-BY-NC-ND 4.0 International license .

395 culture medium, with more than 98% of purity at the end of the downstream process
396 (Fig. 2 and 3).

397 ***3.3. ESI-MS analysis for determining the accurate molecular mass, the verification***
398 ***of the amino sequence and the assessment of disulfide bonds of the***
399 ***deglycosylated C-RBD-H6 PP protein***

400 The C-RBD-H6 PP protein deglycosylated with PNGase-F was analyzed by ESI-MS
401 and the multiply charged spectrum is shown in Fig. 4.A. Deconvolution of this ESI-MS
402 spectrum (Fig. 4.B) showed a very intense signal at 26069.54 Da. This molecular mass
403 agrees very well with the calculated molecular mass (26069.87 Da) for the C-RBD-H6
404 PP considering the presence of four intramolecular disulfide bonds and the two out the
405 three potential N-glycosylation sites transformed into Asp residues due to the action of
406 PNGase-F. Also a low-abundance signal (see star in Fig. 4.B) indicates that a minor
407 fraction of this molecule is devoid of the extension of four N-terminal amino acids (-
408 NSWF) not belonging to the RBD protein.

409 To verify the amino acid sequence as well as the disulfide bonds the deglycosylated
410 protein was digested with trypsin using an in-solution buffer-free digestion protocol
411 developed in our group [16;20]. ESI-MS analysis of the tryptic peptides is shown in Fig.
412 4.C. Full-sequence coverage of C-RBD-H6 PP was verified and the assignment for
413 signals observed in this mass spectrum is summarized in Table 1. ESI-MS/MS analysis
414 of the signal detected at *m/z* 1399.64, 4+ confirmed that Asn^{331} and Asn^{343} (two out the
415 three potential N-glycosylation sites) were transformed into Asp residues by the action
416 of PNGase F (see underlined residues in the Table). The four disulfide bonds (C_{336}-C_{361},
417 C_{379}-C_{432}, C_{391}-C_{525} and C_{480}-C_{488}) present in the native S protein of SARS-CoV-2 were

medRxiv preprint doi: https://doi.org/10.1101/2021.06.29.21259605; this version posted July 3, 2021. The copyright holder for this preprint (which was not certified by peer review) is the author/funder, who has granted medRxiv a license to display the preprint in perpetuity. It is made available under a CC-BY-NC-ND 4.0 International license .

418 also detected in this ESI-MS spectrum (Fig. 4.C and Table 1). Tryptic peptides
419 containing free cysteine residues and S-S scrambling variants were not detected.

420 ESI-MS analysis of the deglycosylated C-RBD-H6 PP protein and its derived tryptic
421 peptides confirmed that N-glycans in its structure increased considerably its molecular
422 mass by SDS-PAGE analysis.

423 ***3.4. Surface Plasmon Resonance characterization of the RBD-ACE2 binding***
424 ***affinity***

425 As shown in Fig. 5, there was no appreciable signal in terms of response units (RU)
426 when measurements were performed a non-related protein used as negative control for
427 BIACORE experiments, immobilizing mFc-ACE2 ligand by Fc region on to a Prot A chip.
428 In contrast, the association rate for C-RBD-H6 PP protein to mFc-ACE2 was 5.4×10^{5} $M^{-1}\cdot s^{-1}$, with a dissociation rate of 7.7×10^{-3} s^{-1}. The equilibrium was reached between 25
430 and 30 seconds, with an estimated dissociation constant of K_D = 14.3×10^{-9} M. The
431 association/dissociation rates as well as K_D were in the expected ranges, according to
432 the previously reported results for the RBD-ACE2 molecular interaction [25].

433 ***3.5. Secondary structure analysis by CD Spectroscopy***

434 Fig. 6 shows the far UV CD spectrum of the C-RBD-H6 PP protein revealing
435 characteristic bands similar to the observed in other recombinant RBD proteins reported
436 previously [8], with maxima at 192 and 231 nm – due to the aromatic contribution - and
437 minimum at 207 nm. Furthermore, as shown in Table 2 the secondary structure content
438 of the protein estimated by BeStSel (7.9% helix, 28.7% beta - antiparallel, relaxed and

medRxiv preprint doi: https://doi.org/10.1101/2021.06.29.21259605; this version posted July 3, 2021. The copyright holder for this preprint
(which was not certified by peer review) is the author/funder, who has granted medRxiv a license to display the preprint in perpetuity.
It is made available under a CC-BY-NC-ND 4.0 International license .

439 right-handed-, 12.9% turn y 50.5% others) is very similar to the values assigned using
440 the 3D coordinates [11]. Moreover, as observed in Fig. 7 the near UV CD spectrum of
441 the protein is well structured, with bands at 263, 269, 277, 281 and 299 nm, indicative of
442 the presence of well-packed aromatic and cysteine residues as expected for a properly
443 folded protein.

444 ***3.6. Antigenicity analysis of C-RBD-H6 PP***

445 To confirm the antigenicity of the yeast-derived protein, several ELISA tests were
446 performed with SS-1, SS-4, SS-7 and SS-8 anti-RBD monoclonal antibodies obtained
447 immunizing with RBD-H6 HEK protein produced in the mammalian cells HEK293T. One
448 of these monoclonal antibodies (SS-8) inhibits the protein binding to the ACE2 receptor
449 with an IC50 of 60 ng/mL. The binding to C-RBD-H6 PP protein was compared to the
450 binding to C-RBD-H6 HEK as shown in Fig. 8.A,E. The reactivity does not differ
451 between the two proteins. Human sera with high neutralization titers for live SARS-CoV-
452 2 viral challenge of Vero E6 cells from eight COVID-19 naturally infected patients and
453 seven individuals that already received Pfizer-BioNTech or Sputnik V complete vaccine
454 schedules were incorporated into the testing panels. None properly folded C-RBD-H6
455 protein produced as inclusion body in BL-21 *E coli* strain was used as a negative
456 control. C-RBD-H6 PP protein obtained from yeast was able to maintain antigenicity
457 comparable to the protein purified from mammalian cells (Fig. 8.B,F and C,G). Minimal
458 signals were detected with the sera from animals immunized with RBD protein
459 expressed in *E. coli*, corroborating the need for a correctly folded protein to ensure the
460 exposition of immunodominant epitopes (data not shown). Further characterization was
461 conducted using polyclonal sera from mice and NHP immunized with C-RBD-H6 PP

medRxiv preprint doi: https://doi.org/10.1101/2021.06.29.21259605; this version posted July 3, 2021. The copyright holder for this preprint
(which was not certified by peer review) is the author/funder, who has granted medRxiv a license to display the preprint in perpetuity.
It is made available under a CC-BY-NC-ND 4.0 International license .

and C-RBD-H6 HEK proteins, and with known capacity to neutralize SARS-CoV-2 infection. All polyclonal sera similarly detect the RBD protein expressed in both heterologous expression system (Fig. 8.D,H).

The C-RBD-H6 PP protein was also used to recall *in vitro* a cellular response in terms of IFNγ secretion using ELISpot from PBMCs of COVID-19 naturally infected subjects with at least three months from hospital release. As shown in Fig. 8.I stimulation with 10 µg/mL of the yeast-produced protein induce IFNγ secretion from COVID-19 naturally infected subjects PBMCs.

3.7. Functionality of yeast-expressed RBD protein

ACE2 receptor binding competition assay

The functionality of the recombinant protein C-RBD-H6 PP was confirmed by the assessment of its ability to bind to the chimeric hFc-ACE2 receptor bound to ELISA plates and also to bind to the ACE2 receptor in Vero E6 cells both in solution or attached to the plate. To evaluate the binding of the protein to hFcACE-2, a serial two-fold dilution curve of the test protein starting from 100 µg/mL was mixed with HEK293T produced hFc-RBD-HRP conjugate at a fixed concentration and added to hFc-ACE2 coated plates. As shown in Fig. 9.A, two independent C-RBD-H6 PP protein preparations effectively displaced the hFc-RBD HEK in the same magnitude that the soluble hFc-ACE2 and the recombinant RBD-H6 HEK protein obtained in HEK293T cells. Two non-related chimeric proteins P64K-VEGFH6 (expressed in *E. coli*), and hFc-VEGFR2 (produced in HEK293T cells) were used as negative controls

medRxiv preprint doi: https://doi.org/10.1101/2021.06.29.21259605; this version posted July 3, 2021. The copyright holder for this preprint (which was not certified by peer review) is the author/funder, who has granted medRxiv a license to display the preprint in perpetuity. It is made available under a CC-BY-NC-ND 4.0 International license .

A similar study was conducted on paraformaldehyde-fixed Vero E6 cells (Fig. 9.B) As expected, no displacement of biotinylated hFc-RBD from the cell membrane was observed in either case using as negative controls the non-related chimeric VEGF protein fused to the N-terminal of *Neisseria meningitidis* (P64K-VEGFH6) or the human Fc (VEGFR2-hFc), and 100 % of the signal was lost when the C-RBD-H6 PP protein, soluble hFc-ACE2 or mFc-ACE2 were added (Fig. 9.C). These results suggest that the yeast-expressed C-RBD-H6 PP protein can bind efficiently to the cell-surface ACE2 receptor.

Further characterization of ACE2 binding was conducted in solution using yeast and mammalian-derived proteins coated in different concentrations in ELISA plates. ACE2 EC-50 on RBD coated plates result in values ranging between 100 and 300 ng/mL in agreement with the values reported for commercial sources of RBD and with our data using RBD variants purified from HEK293T supernatant. Using the same system stability of the protein was verified by incubating the protein at 4 °C, 37 °C, and 50 °C for 2 h without significant loss in ACE2 binding activity (data not shown)

These results confirm the specific binding of the yeast-expressed RBD with SARS-CoV-2 receptor ACE2 either cell-bound or soluble, indicating that the antigen herein obtained is functional.

Yeast-expressed RBD protein elicited RBD-ACE2 receptor binding inhibition and SARS-CoV-2 neutralizing antibodies in rodents and NHP

To evaluate the immunogenicity of C-RBD-H6 PP protein, BALB/c mice were immunized thrice at 7 days intervals by the intraperitoneal route with 50µg of the

medRxiv preprint doi: https://doi.org/10.1101/2021.06.29.21259605; this version posted July 3, 2021. The copyright holder for this preprint
(which was not certified by peer review) is the author/funder, who has granted medRxiv a license to display the preprint in perpetuity.
It is made available under a CC-BY-NC-ND 4.0 International license .

505 protein. The IgG antibody response in mice at days 21 and 35 shows that the C-RBD-
506 H6 PP protein was able to induce antibody responses in ELISA coated with the RBD
507 protein produced in mammalian HEK293T cells. Seroconversion was achieved a week
508 after the first boost (Fig. 10.A). The administration of a second booster at day 21
509 significantly increases both RBD-specific IgG titers and the inhibitory potential of the
510 sera to reduce the protein binding to its cognate receptor ACE2 a fact that correlates
511 with live SARS-CoV-2 neutralization (Fig. 10.B,C).

512 The C-RBD-H6 PP protein was also tested in SD rats using intramuscular
513 administration of 9 µg every 7 days for 10 weeks. Assessment of IgG and RBD-ACE2
514 receptor binding inhibition three days after the last immunization indicates high RBD-
515 specific antibody titers that correlate with the inhibitory titer. The former also display a
516 high correlation with the neutralization titer of live SARS-CoV-2 virus in Vero E6 cells
517 (Fig. 10.D,F).

518 The C-RBD-H6 PP protein evaluation in NHP using short intramuscular administration
519 schedule on days 0-14-28, and two dose levels indicate a dose-response effect with
520 seroconversion of 83 % (5 of 6 animals) and 100% (the 10 animals) for the 50 µg and
521 100 µg dose respectively after the first booster and a 100 % seroconversion in both
522 schedules after the second booster. Total IgG titers increased to 44,240 StdU/mL and
523 62,435 StdU/mL respectively for monkeys included in the low and high-dose groups. In
524 both cases, the titers were significantly higher than those detected in the convalescent
525 panel of sera. The geometric median ACE2 binding inhibition titer for 50 µg dose was
526 1:230, while a significantly higher value of 1:705 was detected for the animals receiving
527 the 100 µg dose. Both values were higher than those detected in a panel of COVID-19

medRxiv preprint doi: https://doi.org/10.1101/2021.06.29.21259605; this version posted July 3, 2021. The copyright holder for this preprint
(which was not certified by peer review) is the author/funder, who has granted medRxiv a license to display the preprint in perpetuity.
It is made available under a CC-BY-NC-ND 4.0 International license .

convalescent subjects ($p<0.001$, Kruskal-Walis). The higher titers for the 100 µg dose correlate with and enhancement in the inhibition of RBD-ACE2 binding for this group. The analysis of the neutralization titer of live SARS-CoV-2 virus in Vero E6 cells corroborates these findings, indicating that 50µg dose is sufficient to induce ACE2 binding inhibition titers with an EC50 geometric mean of 1:66 serum dilution, a value 6 times higher than the reported for the convalescent panel. A significant increase to 1:141 in this parameter was detected for the 100 µg dose pointing to a dose-related effect (Fig. 10.G,J).

The specific IgG antibody and the inhibition of RBD-ACE2 binding were only detected in C-RBD-H6 PP protein-inoculated animals but not in control animals. The immune responses evidenced the boosting effect and the specific dose-dependent effect, as compare to negative results for control animals.

Cellular response

Cellular response recall was evaluated three months after the last immunization in BALB/c mice receiving subcutaneous doses of 25 µg in alum in a 0-14-35 days schedule. The evaluation of the presence of a memory response in the animal's spleens indicates a significant induction of clones secreting IFNγ in response to incubation with the C-RBD-H6 PP antigen. Furthermore, the analyses of the supernatant of the recall reaction point to the predominant induction of IFNγ followed by IL-2, IL-6 and to a lower extend TNFα and IL-4 (Fig. 11). Our findings in the systemic compartment (Fig. 11.A) were similar to those found for CD3+ cells enriched from mice lungs (Fig. 11.B),

medRxiv preprint doi: https://doi.org/10.1101/2021.06.29.21259605; this version posted July 3, 2021. The copyright holder for this preprint
(which was not certified by peer review) is the author/funder, who has granted medRxiv a license to display the preprint in perpetuity.
It is made available under a CC-BY-NC-ND 4.0 International license .

549 indicating that the response can also be recalled in the organ primarily affected by
550 SARS-CoV-2 infection.

551 **4. Discussion**

552 Despite the impressive development of prophylactic vaccines against COVID-19 and
553 that several vaccines have reached the Emergency Use Authorization or
554 Pharmaceutical Registry, there is not a sufficient supply of vaccines. In addition, the
555 challenge of the continuous emergence of new mutant strains of the virus will require
556 updating the antigen sequences included in the vaccines and administer booster doses
557 to maintain the immunity of the population.

558 Results from this study demonstrate that it is possible to develop a vaccine candidate
559 expressing RBD protein of SARS-CoV-2 using the yeast *P. pastoris*. The RBD was
560 selected base on the state of the art evidence of the main contribution of the epitopes of
561 RBD to the neutralization activity of the sera [13;26-28]

562 Moreover neutralizing antibody responses generated after immunization with Pfizer-
563 BioNtech or Moderna vaccines of previously infected subjects, are mainly due to anti-
564 RBD antibodies. The sera depletion of antibodies targeting the RBD abrogates sera
565 neutralization capacity [29]

566 Optimal conditions for the production of a recombinant protein in *P. pastoris* expression
567 system differ according to the target protein. Indeed, we were able to obtain 30-40 mg/L
568 of the RBD with more than 98% of purity, close to the yield obtained in previous report
569 by Arbeitman C.R., et al [8], an essential condition to develop a vaccine candidate. In
570 addition to the protein yield, it is important the sugar composition. In *P. pastoris* the

medRxiv preprint doi: https://doi.org/10.1101/2021.06.29.21259605; this version posted July 3, 2021. The copyright holder for this preprint
(which was not certified by peer review) is the author/funder, who has granted medRxiv a license to display the preprint in perpetuity.
It is made available under a CC-BY-NC-ND 4.0 International license .

571 glycosylation pattern is characterized by the high mannose content. Mannosylation
572 enhances activation of antigen-presenting cells like macrophages and dendritic cells,
573 functioning as immunopotentiator while increases the antigen immunogenicity
574 compared with its nonglycosylated counterparts [30]. The ionic interactions dependent
575 on sugar composition also could help to stabilize RBD structure.

576 Our results on the affinity of the *P. pastoris* recombinant protein C-RBD-H6 PP by the
577 receptor comply with those of other authors performing binding assays in BIACORE for
578 the interaction pair RBD-ACE2 [31-33]. It means that probably the subunit vaccine
579 based on C-RBD-H6 PP may elicit an effective antibody response against SARS-CoV-
580 2, avoiding the virus entry and replication by blocking RBD-ACE2 interaction in real
581 SARS-CoV-2 infection context.

582 The correct glycosylated protein during the transit in the endoplasmic reticulum and
583 Golgi apparatus, go to the secretory pathway. If the protein is unable to fold properly is
584 degraded in the cytosol. This mechanism guarantees that only properly folded proteins
585 are secreted [8;34]. Our results demonstrated the presence of four intramolecular
586 disulfide bonds identical to those present in the native RBD of SARS-CoV-2. These
587 results as well as the secondary structure determined by CD spectroscopy confirm the
588 right folding of the C-RBD-H6 PP.

589 Remarkably despite the known difference in the sugar composition of the protein
590 expressed in *P. pastoris* compared to the expression systems in mammals, the
591 antigenicity of the protein is similar both with polyclonal sera from mice and monkeys
592 immunized with the recombinant protein, such as with human sera from individuals with
593 natural coronavirus infection or vaccinated with the Pfizer-BioNTech or Sputnik V

medRxiv preprint doi: https://doi.org/10.1101/2021.06.29.21259605; this version posted July 3, 2021. The copyright holder for this preprint
(which was not certified by peer review) is the author/funder, who has granted medRxiv a license to display the preprint in perpetuity.
It is made available under a CC-BY-NC-ND 4.0 International license .

vaccines against SARS-CoV-2. The C-RBD-H6 PP protein also stimulated cellular response mediated by IFNγ secretion in lymphocytes isolated from convalescent subjects. The C-RBD-H6 PP protein also inhibited the RBD binding to the ACE2 receptor in a competitive ELISA regardless of whether the RBD receptor was obtained recombinant or it is found directly in the membrane of Vero E6 cells. In the same manner, the sera from mice, rats and NHP immunized with C-RBD-H6 PP protein inhibited the RBD-ACE2 receptor binding and neutralize the SARS-CoV-2 in microneutralization tests.

The need for the accelerated development of the vaccine candidate during the pandemic, led to the neutralizing activity of the NHP sera being evaluated just one week after the third dose, reaching titers comparable to the panel of convalescent sera used as a control. It is known that a long time for bleeding would lead to the maturation and selection of B cell clones producing high avidity antibodies and consequently higher neutralizing titers.

Conclusions

Optimal conditions for the production of a recombinant protein in *P. pastoris* expression system differ according to the target protein. Indeed, we were able to obtain 30-40 mg/L of the RBD with more than 98% of purity.

Our ESI-MS results demonstrated the presence of four intramolecular disulfide bonds identical to those present in the native RBD of SARS-CoV-2, and the CD spectrum of the protein indicates the presence of well-packed aromatic and cysteine residues. These results together with the high receptor binding affinity in BIACORE assays confirm the right folding of the C-RBD-H6 PP protein.

medRxiv preprint doi: https://doi.org/10.1101/2021.06.29.21259605; this version posted July 3, 2021. The copyright holder for this preprint (which was not certified by peer review) is the author/funder, who has granted medRxiv a license to display the preprint in perpetuity. It is made available under a CC-BY-NC-ND 4.0 International license .

The C-RBD-H6 PP antigenicity and the capacity of the sera from immunized mice, rats and NHP to inhibited the RBD-ACE2 receptor binding and neutralize the live virus infection to Vero E6 cells, points to the feasibility of the protein as a vaccine candidate.

Funding

This work was supported with funds from the BioCubaFarma, the Center for Genetic Engineering and Biotechnology, and by the Grant of the National Science and Technology Program - Biotechnology, Pharmaceutical Industry and Medical Technologies, of the Ministry of Science and Technology, project code PN385LH007-048. The Civilian Defense Scientific Research Center supported the microneutralization assays.

Authors Contributions

GGN: provided original ideas and study concept and design, data curation, analysis and interpretation of data, and drafting, review and editing of the final version of the manuscript and studies supervision. MLF: contributed to analysis and interpretation of data, study design, review of the manuscript and studies supervision. LJGL: contributed to ESI-MS study design, acquisition of data, analysis and interpretation of data, and drafting and review of the manuscript. LAER, IAM and YRG: performed the ESI-MS studies, acquisition of data, analysis and interpretation of data. GCH: performed glycosylation studies. ACR: performed drafting and execution of Biacore studies. GMP: performed the protein purification studies. MPI and JZS: performed fermentation studies. GCS: provided original idea and drafting of the genetic construction, and performed structural analysis experiments by CD spectroscopy. AMMD: provided original ideas and performed the genetic construction and review of the manuscript. and

medRxiv preprint doi: https://doi.org/10.1101/2021.06.29.21259605; this version posted July 3, 2021. The copyright holder for this preprint (which was not certified by peer review) is the author/funder, who has granted medRxiv a license to display the preprint in perpetuity. It is made available under a CC-BY-NC-ND 4.0 International license .

DGR: performed the genetic construction and protein expression experiments. MBR: provided original ideas, study designs, analysis and interpretation of data, drafting and review of the manuscript, graphic and statistical processing and execution of antigenicity, immunogenicity and cellular response studies. IGM and CCHA: performed antigenicity, immunogenicity studies and analysis of cellular response in mouse, rat, and NHP. OCS: study design and supervision of the microneutralization experiments. GLP: contributed to analytical procedures and donor patients selection and evaluation of the immunological and functional response. JVH, EMD, EPV and MAA: study concept and supervision.

Disclosure

MLF, MBR, AMMD, DGR, ACR, GCS, GMP, EPV, MAA and GGN are co-authors of the Center for Genetic Engineering and Biotechnology patent application comprising the C-RBD-H6 PP protein as a vaccine antigen against SASR-CoV-2.

All authors approved integrally the final article.

Acknowledgment

The authors acknowledge Dr. Gabriel Padron and Dr. Diana Garcia del Barco Herrera for their writing assistance. We also thank Dr. Gertrudis Rojas, Dr. Tays Hernández and Dr. Belinda Sanchez from the Center for Molecular Immunology for the recombinant mFc-RBD and hFc-RBD chimeric proteins.

medRxiv preprint doi: https://doi.org/10.1101/2021.06.29.21259605; this version posted July 3, 2021. The copyright holder for this preprint
(which was not certified by peer review) is the author/funder, who has granted medRxiv a license to display the preprint in perpetuity.
It is made available under a CC-BY-NC-ND 4.0 International license .

Figure Legends

Fig. 1. Analysis of culture supernatants from randomly selected RBD-secreting *P. pastoris* clones. In all cases 10 µL of each sample were analyzed under reducing conditions. Panel A: Coomassie Blue-stained 12.5 % SDS-PAGE; panel B: Western blotting of an identical gel with an anti-His tail antibody. Lane V: Strain transformed with the empty vector. Lanes A, B and C: clones transformed with the RBD plasmid.

Fig. 2. RP-HPLC. Analysis of C-RBD-H6 PP protein produced in *Pichia pastoris*, with 98.6 % of purity; analyzed on a reversed phase C8 Vydac analytical column. The gradient is shown with a blue line.

Fig. 3. **Protein electrophoresis.** Coomassie Blue stained 12,5 % SDS-PAGE gel of 10 µg of the purified C-RBD-H6 PP under reducing conditions. Lane 1: C-RBD-H6 PP protein; Lane 2 Molecular weight markers.

Fig. 4. ESI-MS spectra. (A) Multiply-charged and (B) deconvoluted ESI-MS spectra of C-RBD-H6 PP protein previously N-deglycosylated with PNGase-F. The parenthesis in **(**B**)** shows the expected molecular mass considering the presence of four intramolecular disulfide bonds and the Asn^{331} and Asn^{343} transformed into Asp residues by the PNGase F during the deglycosylation step. (C) ESI-MS spectrum of the tryptic peptides generated by an in-solution buffer-free trypsin digestion protocol of the N-deglycosylated C-RBD-H6 PP protein. The star in (B) and (C) indicates the low-abundance species that do not contain the four residues (-NWSF) located at the N-terminal end. Nt and Ct-His_6 represents the N-terminal end and the His_6-tag C-terminal end peptides of C-RBD-H6 PP protein, respectively.

medRxiv preprint doi: https://doi.org/10.1101/2021.06.29.21259605; this version posted July 3, 2021. The copyright holder for this preprint
(which was not certified by peer review) is the author/funder, who has granted medRxiv a license to display the preprint in perpetuity.
It is made available under a CC-BY-NC-ND 4.0 International license .

682 **Fig. 5. SPR analysis from C-RBD-H6 PP protein obtained in *P. pastoris* interacting**
683 **with mFc-ACE2 receptor in a single-cycle BIACORE experiment**. (A) Sensorgrams
684 corresponding to one of the replicates of the protein dissolved in PBS, pH = 7.2, (B)
685 Non-related protein (also expressed in yeast), used as negative control for the
686 interaction with immobilized mFc-ACE2 cell receptor. As expected, there were no
687 significant signals for the protein used as negative control; compared to the curves
688 obtained for C-RBD-H6 PP protein in the same experimental conditions (similar axis
689 scale is shown).

690 **Fig. 6. Far UV CD spectrum of the C-RBD-H6 PP protein**.

691 **Fig. 7**. **Near UV CD spectrum of the C-RBD-H6 PP protein**. Bands at 263, 269, 277,
692 281 and 299 nm, indicate the presence of well packed aromatic and cystine residues.

693 **Fig. 8**. **Antigenicity of the RBD protein produced in *P. pastoris* yeast**. C-RBD-H6
694 PP (upper panel) or RBD-H6 HEK (lower panel) proteins were used for coating ELISA
695 plates and for animal immunization. Sera and monoclonal antibodies were used in serial
696 two-fold dilutions. (A,E). SS-1, SS4, SS-7 and SS-8 monoclonal antibodies; (B,F).
697 COVID-19 sera from convalescents; (C,G) Sera from subjects immunized with Pfizer-
698 BioNTech (red squares) and Sputnik vaccines (black triangles); (D,H). Mice (grey) and
699 NHP (blue) sera; (**I**). C-RBD-H6 PP stimulates INFγ secretion in CD3+ cells from
700 naturally infected individuals. Wilcoxon matched paired test.

701 **Fig. 9**. **Binding inhibition capacity of two independent protein preparations of the**
702 **C-RBD-H6 PP (L04 and L07)**. (A). The C-RBD-H6 PP protein displaced the hFc-RBD-
703 HRP from the hFc-ACE2 coated ELISA plates, and (B) from the ACE2 receptor in Vero
704 E6 cells. (C). The C-RBD-H6 PP protein was recognized by the soluble ACE2 receptor.

medRxiv preprint doi: https://doi.org/10.1101/2021.06.29.21259605; this version posted July 3, 2021. The copyright holder for this preprint
(which was not certified by peer review) is the author/funder, who has granted medRxiv a license to display the preprint in perpetuity.
It is made available under a CC-BY-NC-ND 4.0 International license .

P64K-VEGFH6 and hFc-VEGFR2 non-related chimeric proteins were used as negative controls.

Fig. 10. **Immunogenicity of C-RBD-H6 PP protein in three animal species using different immunization routes and schedules**. (A) Evaluation of RBD-specific IgG in BALB/c mice 7 days after second and third intra-peritoneal immunization (n=10); (B). Evaluation in BALB/c mice of EC50 for the ACE2 binding inhibition and PRNT in the microneutralization assay (n=10); C. Correlation analyses of the ACE2 binding inhibition and microneutralization tests in mice (C). Sperman, r=0.6482, p=0.0478); (D). Evaluation of RBD-specific IgG in SD rats 3 days after 10 weakly subcutaneous immunization (n=10); (E). Evaluation in SD rats of EC50 for the ACE2 binding inhibition and PRNT in the microneutralization assay (n=20); (F). Correlation analyses of the ACE2 binding inhibition and microneutralization tests in rats (Spearman, r=0.9233, p=< 0.0001); (G). Evaluation of RBD specific IgG in NHP with 50 µg and 100 µg dose 14 days after three subcutaneous immunizations every second week with 6 and 10 animals respectively; (H). Evaluation in NHP of EC50 for the ACE2 binding inhibition; (I). Evaluation in NHP of EC50 for the PRNT in the microneutralization assay. (J). Association Correlation analyses of the Inhibition and microneutralization tests in NHP (Spearman, r=0.8994, p<0.0001).

Fig. 11. **Heatmap of the cytokine response**. Splenocytes (A) and Lung CD3+ enriched cells (B), after restimulation with C-RBD-H6 PP. Cells were obtained three months after the last immunization, from 4 to 5 mice per group that received three subcutaneous 25 µg doses. Non-stimulated controls were subtracted from re-stimulated samples.

medRxiv preprint doi: https://doi.org/10.1101/2021.06.29.21259605; this version posted July 3, 2021. The copyright holder for this preprint (which was not certified by peer review) is the author/funder, who has granted medRxiv a license to display the preprint in perpetuity. It is made available under a CC-BY-NC-ND 4.0 International license .

728 **Table 1.** Summary for the sequence verification of the N-deglycosylated C-RBD-H6 PP
729 considering the ESI-MS analysis of tryptic peptides generated by the in-solution buffer-
730 free digestion.

731

Code[a)]	m/z_{Theor}	z	m/z_{Exp}	Assignment
C^{336}-C^{361}, Nt	1399.64	4	1399.63	*NWSFFSNIGGSSGGS*-^{331}DITNLCPFGEVFDATR^{346} b) / ^{358}ISNCVADYSVLYNSASFSTFK^{378} (Native C^{336}-C^{361}, N-terminal end, Asn^{331} and Asn^{343}→Asp)
C^{336}-C^{361}, Nt-NWSF	1266.09	4	1266.07	*FSNIGGSSGGS*-^{331}DITNLCPFGEVFDATR^{346} b) / ^{358}ISNCVADYSVLYNSASFSTFK^{378} (Native C^{336}-C^{361}, N-terminal end -NWSF, Asn^{331} and Asn^{343}→Asp corresponding to the two N-glycosylation sites)
F^{347}-R^{355}	557.28	2	557.26	^{347}FASVYAWNR^{355}
K^{356}-R^{357}	303.21	1	303.20	^{356}KR^{357}
C^{379}-C^{432}	1020.81 765.86	3 4	1020.79 765.85	^{379}CYGVSPTK^{386} | ^{425}LPDDFTGCVIAWNSNNLDSK^{444} (Native C^{379}-C^{432})
C^{379}*-C^{432}	982.71	4	982.69	^{64}CYGVSPTK^{71} | ^{418}IADYNYKLPDDFTGCVIAWNSNNLDSK^{444} (Native C^{379}-C^{432}, 1 missed cleavage)
C^{391}-C^{525}	992.52	4	992.47	^{387}LNDLCFTNVYADSFVIR^{403} | ^{510}VVVLSFELLHAPATVCGPK^{528} (Native C^{391}-C^{525})
G^{404}-R^{408}	575.28	1	575.27	^{404}GDEVR^{408}
Q^{409}-K^{417}	450.25	2	450.24	^{409}QIAPGQTGK^{417}
I^{418}-K^{424}	443.72	2	443.71	^{418}IADYNYK^{424}

medRxiv preprint doi: https://doi.org/10.1101/2021.06.29.21259605; this version posted July 3, 2021. The copyright holder for this preprint (which was not certified by peer review) is the author/funder, who has granted medRxiv a license to display the preprint in perpetuity. It is made available under a CC-BY-NC-ND 4.0 International license .

V^{445}-R^{454}	609.80	2	609.78	^{445}VGGNYNYLYR^{454}
L^{455}-R^{457}	435.27	1	435.26	^{455}LFR^{457}
S^{459}-R^{466}	495.77	2	495.76	^{459}SNLKPFER^{466}
C^{480}-C^{488}	1589.38 1192.29	3 4	1589.35 1192.26	^{467}DISTEIYQAGSTPCNGVEGFNCYFPLQSYGFQPTNGVGYQP YR^{509} |_____| (Native C^{480}-C^{488})
Ct*-His_6	799.68 600.01	3 4	799.67 600.00	^{529}K-*GGSGGSSSSSSSSSSIEHHHHHH* [b)] (C-terminal end, 1 missed cleavage)
Ct-His_6	756.98 567.99	3 4	756.97 567.98	*GGSGGSSSSSSSSSSIEHHHHHH* [b)] (C-terminal end)

Nt: N-terminal end, Ct-His_6: His-tag C-terminal end. $C^{\#}$-$C^{\#}$ corresponds to tryptic peptides linked either by intermolecular disulfide bonds or a tryptic peptide that contains an intramolecular disulfide bond in its structures.

m/z_{calc} correspond to the calculated m/z values for all tryptic peptides generated by the in-solution buffer-free digestion of the N-deglycosylated protein.

m/z_{exp} correspond to the experimental m/z values for all tryptic peptides observed in the ESI-MS analysis shown in Fig. 4.C.

Regions of the sequence written in italic do not correspond to the RBD of SRAS-CoV-2 and were inserted in the cloning stage, while underlined residues indicate the conversion of N-glycosylated asparagines (Asn^{331} and Asn^{343}) into aspartic acid residues by the action of PNGase-F (Asn^{331} and Asn^{343}→Asp).

medRxiv preprint doi: https://doi.org/10.1101/2021.06.29.21259605; this version posted July 3, 2021. The copyright holder for this preprint (which was not certified by peer review) is the author/funder, who has granted medRxiv a license to display the preprint in perpetuity. It is made available under a CC-BY-NC-ND 4.0 International license .

745 **Table 2.** Secondary structure content of the protein estimated by CD (BeStSel) and 3D

746 coordinates (DSSP)

747

Secondary Structure Element	Secondary Structure Content, %	
	Method	
	BeStSel	DSSP
Helix	7.9	9.3
Beta antiparallel	28.7	22.4
Beta parallel	0.0	0.0
Turn	12.9	22.4
others	50.5	45.9
Helix1 (regular)	3.3	-
Helix2 (distorted)	4.6	-
Beta Antiparallel_1 (left-handed)	0.9	-
Beta Antiparallel_2 (relaxed)	12.0	-
Beta Antiparallel_3 (right-handed)	15.8	-

748

medRxiv preprint doi: https://doi.org/10.1101/2021.06.29.21259605; this version posted July 3, 2021. The copyright holder for this preprint
(which was not certified by peer review) is the author/funder, who has granted medRxiv a license to display the preprint in perpetuity.
It is made available under a CC-BY-NC-ND 4.0 International license .

Reference List

[1] Pentón-Arias E, Muzio V., González-Griego M. The hepatitis B virus (HBV) infection and its prevention by a recombinant-DNA viral surface antigen (rec-HBsAg) vaccine. Biotecnología Aplicada 1994;11(1):1-11.

[2] Hardy E, Martínez E, Diago D, Díaz R, González D, herrera L. Large-scale Production of recombinant Hepatitis B Surface Antigen from Pichia pastoris. Biotecnología Aplicada 2000;17(1):52.

[3] Hernandez-Bernal F, Aguilar-Betancourt A, Aljovin V, et al. Comparison of four recombinant hepatitis B vaccines applied on an accelerated schedule in healthy adults. Hum Vaccin 2011 Oct;7(10):1026-36.

[4] Ministry of Public Health of Cuba. Statistical Yearbook. Infomed 2020Available from: URL: https://files.sld.cu/bvscuba/files/2020/05/Anuario-Electr%c3%b3nico-Espa%c3%b1ol-2019-ed-2020.pdf

[5] Kodati B, Darbha S. Mammalian Expression System and Improvisation for High Production. International Journal of Science and Research 2016;5(6):743-9.

[6] Barone PW, Wiebe ME, Leung JC, et al. Viral contamination in biologic manufacture and implications for emerging therapies. Nat Biotechnol 2020 May;38(5):563-72.

medRxiv preprint doi: https://doi.org/10.1101/2021.06.29.21259605; this version posted July 3, 2021. The copyright holder for this preprint
(which was not certified by peer review) is the author/funder, who has granted medRxiv a license to display the preprint in perpetuity.
It is made available under a CC-BY-NC-ND 4.0 International license .

768 [7] Rosano GL, Ceccarelli EA. Recombinant protein expression in Escherichia coli:
769 advances and challenges. Front Microbiol 2014;5:172.

770 [8] Arbeitman CR, Auge G, Blaustein Ma, et al. Structural and functional comparison
771 of SARS-CoV-2-spike receptor binding domain produced in Pichia pastoris and
772 mammalian cells. Scientific Reports 2020;10(1):21779.

773 [9] Karbalaei M, Rezaee SA, Farsiani H. Pichia pastoris: A highly successful
774 expression system for optimal synthesis of heterologous proteins. J Cell Physiol
775 2020 Sep;235(9):5867-81.

776 [10] Daly R, Hearn MT. Expression of heterologous proteins in Pichia pastoris: a useful
777 experimental tool in protein engineering and production. J Mol Recognit 2005
778 Mar;18(2):119-38.

779 [11] Wrapp D, Wang N, Corbett KS, et al. Cryo-EM Structure of the 2019-nCoV Spike
780 in the Prefusion Conformation. bioRxiv 2020 Feb 15.

781 [12] Grant OC, Montgomery D, Ito K, Woods RJ. Analysis of the SARS-CoV-2 spike
782 protein glycan shield reveals implications for immune recognition. Sci Rep 2020
783 Sep 14;10(1):14991.

medRxiv preprint doi: https://doi.org/10.1101/2021.06.29.21259605; this version posted July 3, 2021. The copyright holder for this preprint
(which was not certified by peer review) is the author/funder, who has granted medRxiv a license to display the preprint in perpetuity.
It is made available under a CC-BY-NC-ND 4.0 International license .

784 [13] Premkumar L, Segovia-Chumbez B, Jadi R, et al. The receptor binding domain of
785 the viral spike protein is an immunodominant and highly specific target of
786 antibodies in SARS-CoV-2 patients. Sci Immunol 2020 Jun 11;5(48).

787 [14] Pollet J, Chen WH, Versteeg L, et al. SARSCoV-2 RBD219-N1C1: A yeast-
788 expressed SARS-CoV-2 recombinant receptor-binding domain candidate vaccine
789 stimulates virus neutralizing antibodies and T-cell immunity in mice. Hum Vaccin
790 Immunother 2021 Apr 13;1-11.

791 [15] Chen WH, Wei J, Kundu RT, et al. Genetic Modification to Design a Stable Yeast-
792 expressed Recombinant SARS-CoV-2 Receptor Binding Domain as a COVID-19
793 Vaccine Candidate. bioRxiv 2021 Jan 1;2020.

794 [16] Espinosa LA, Ramos Y, Andújar I, et al. In-solution buffer-free digestion for the
795 analysis of SARS-CoV-2 RBD proteins allows a full sequence coverage and
796 detection of post-translational modifications in a single ESI-MS spectrum. bioRxiv
797 2021 Jan 1;2021.

798 [17] Grote A, Hiller K, Scheer M, et al. JCat: a novel tool to adapt codon usage of a
799 target gene to its potential expression host. Nucleic Acids Res 2005 Jul 1;33(Web
800 Server issue):W526-W531.

medRxiv preprint doi: https://doi.org/10.1101/2021.06.29.21259605; this version posted July 3, 2021. The copyright holder for this preprint
(which was not certified by peer review) is the author/funder, who has granted medRxiv a license to display the preprint in perpetuity.
It is made available under a CC-BY-NC-ND 4.0 International license .

[18] Higgins DR, Busser K, Comiskey J, Whittier PS, Purcell TJ, Hoeffler JP. Small vectors for expression based on dominant drug resistance with direct multicopy selection. Methods Mol Biol 1998;103:41-53.

[19] Gurramkonda C, Polez S, Skoko N, et al. Application of simple fed-batch technique to high-level secretory production of insulin precursor using Pichia pastoris with subsequent purification and conversion to human insulin. Microb Cell Fact 2010 May 12;9:31.

[20] Betancourt LH, Espinosa LA, Ramos Y, et al. Targeting the hydrophilic regions of recombinant proteins by MS via in-solution buffer-free trypsin digestion. Eur J Mass Spectrom (Chichester) 2020 Jun;26(3):230-7.

[21] Micsonai A, Wien F, Kernya L, et al. Accurate secondary structure prediction and fold recognition for circular dichroism spectroscopy. Proc Natl Acad Sci U S A 2015 Jun 16;112(24):E3095-E3103.

[22] Micsonai A, Bulyaki E, Kardos J. BeStSel: From Secondary Structure Analysis to Protein Fold Prediction by Circular Dichroism Spectroscopy. Methods Mol Biol 2021;2199:175-89.

[23] Kabsch W, Sander C. Dictionary of protein secondary structure: pattern recognition of hydrogen-bonded and geometrical features. Biopolymers 1983 Dec;22(12):2577-637.

medRxiv preprint doi: https://doi.org/10.1101/2021.06.29.21259605; this version posted July 3, 2021. The copyright holder for this preprint
(which was not certified by peer review) is the author/funder, who has granted medRxiv a license to display the preprint in perpetuity.
It is made available under a CC-BY-NC-ND 4.0 International license .

[24] Vriend G. WHAT IF: a molecular modeling and drug design program. J Mol Graph 1990 Mar;8(1):52-6, 29.

[25] Wang Q, Zhang Y, Wu L, et al. Structural and Functional Basis of SARS-CoV-2 Entry by Using Human ACE2. Cell 2020 May 14;181(4):894-904.

[26] Suthar MS, Zimmerman MG, Kauffman RC, et al. Rapid Generation of Neutralizing Antibody Responses in COVID-19 Patients. Cell Rep Med 2020 Jun 23;1(3):100040.

[27] Robbiani DF, Gaebler C, Muecksch F, et al. Convergent antibody responses to SARS-CoV-2 in convalescent individuals. Nature 2020 Aug;584(7821):437-42.

[28] Piccoli L, Park YJ, Tortorici MA, et al. Mapping Neutralizing and Immunodominant Sites on the SARS-CoV-2 Spike Receptor-Binding Domain by Structure-Guided High-Resolution Serology. Cell 2020 Nov 12;183(4):1024-42.

[29] Goel RR, Apostolidis SA, Painter MM, et al. Distinct antibody and memory B cell responses in SARS-CoV-2 naive and recovered individuals following mRNA vaccination. Sci Immunol 2021 Apr 15;6(58).

[30] Luong M, Lam JS, Chen J, Levitz SM. Effects of fungal N- and O-linked mannosylation on the immunogenicity of model vaccines. Vaccine 2007 May 30;25(22):4340-4.

medRxiv preprint doi: https://doi.org/10.1101/2021.06.29.21259605; this version posted July 3, 2021. The copyright holder for this preprint
(which was not certified by peer review) is the author/funder, who has granted medRxiv a license to display the preprint in perpetuity.
It is made available under a CC-BY-NC-ND 4.0 International license .

838 [31] Shang J, Ye G, Shi K, et al. Structural basis of receptor recognition by SARS-CoV-
839 2. Nature 2020 May;581(7807):221-4.

840 [32] Lan J, Ge J, Yu J, et al. Structure of the SARS-CoV-2 spike receptor-binding
841 domain bound to the ACE2 receptor. Nature 2020 May;581(7807):215-20.

842 [33] Sui J, Deming M, Rockx B, et al. Effects of human anti-spike protein receptor
843 binding domain antibodies on severe acute respiratory syndrome coronavirus
844 neutralization escape and fitness. J Virol 2014 Dec;88(23):13769-80.

845 [34] D'Alessio C, Caramelo JJ, Parodi AJ. UDP-GlC:glycoprotein glucosyltransferase-
846 glucosidase II, the ying-yang of the ER quality control. Semin Cell Dev Biol 2010
847 Jul;21(5):491-9.

848

849

medRxiv preprint doi: https://doi.org/10.1101/2021.06.29.21259605; this version posted July 3, 2021. The copyright holder for this preprint
(which was not certified by peer review) is the author/funder, who has granted medRxiv a license to display the preprint in perpetuity.
It is made available under a CC-BY-NC-ND 4.0 International license .

Appendix. Other co-authors in the Study

Center for Genetic Engineering and Biotechnology

Isela María Garcia Tamayo

Yahima Chacón Quintero

Ricardo Ulises Martinez Rosales

Dionne Casillas Casanova

Ailyn de la Caridad Ramón Sánchez

Lizet Aldana Velazco

Jorge Castro Velazco

Civilian Defense Scientific Research Center

Juliet María Enriquez Puertas, M.Sc.

Mireida Rodríguez Acosta, M.D., Ph.D.

Enrique Noa Romero, Ph.D.

Nibaldo Luis González Sosa, M.Sc.

Marta Dubed Echevarría, M.Sc.

medRxiv preprint doi: https://doi.org/10.1101/2021.06.29.21259605; this version posted July 3, 2021. The copyright holder for this preprint
(which was not certified by peer review) is the author/funder, who has granted medRxiv a license to display the preprint in perpetuity.
It is made available under a CC-BY-NC-ND 4.0 International license .

866

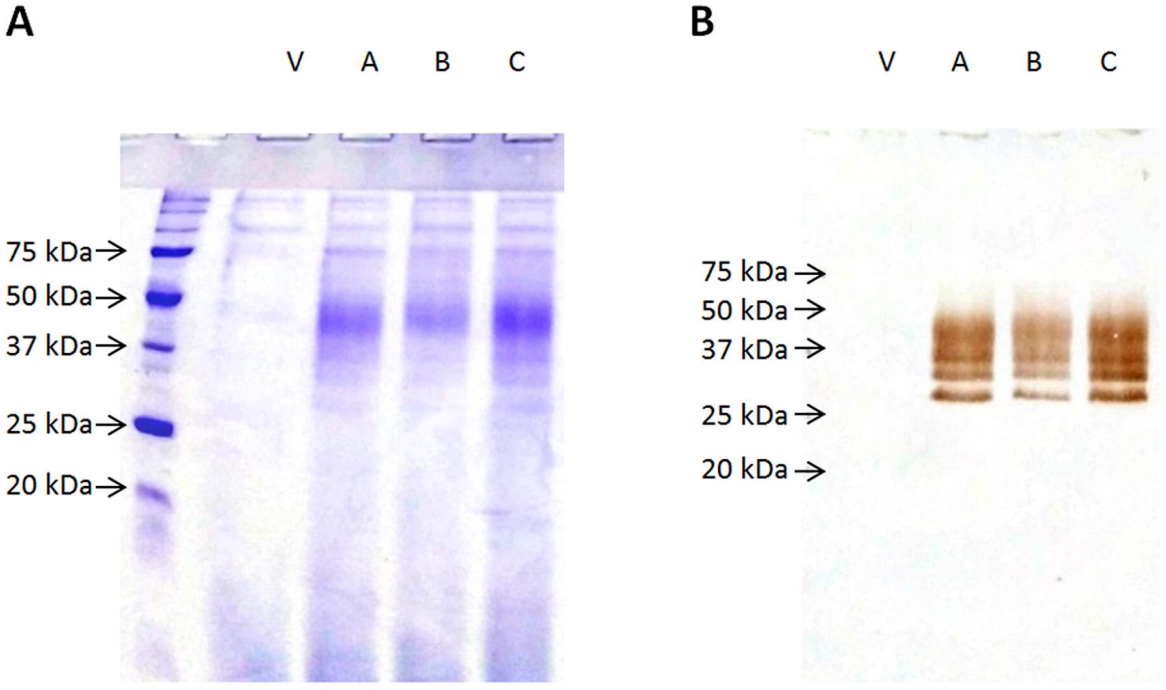
A
V
A
B
C
75 kDa
50 kDa
37 kDa
25 kDa
20 kDa
B
V
A
B
C
75 kDa
50 kDa
37 kDa
25 kDa
20 kDa

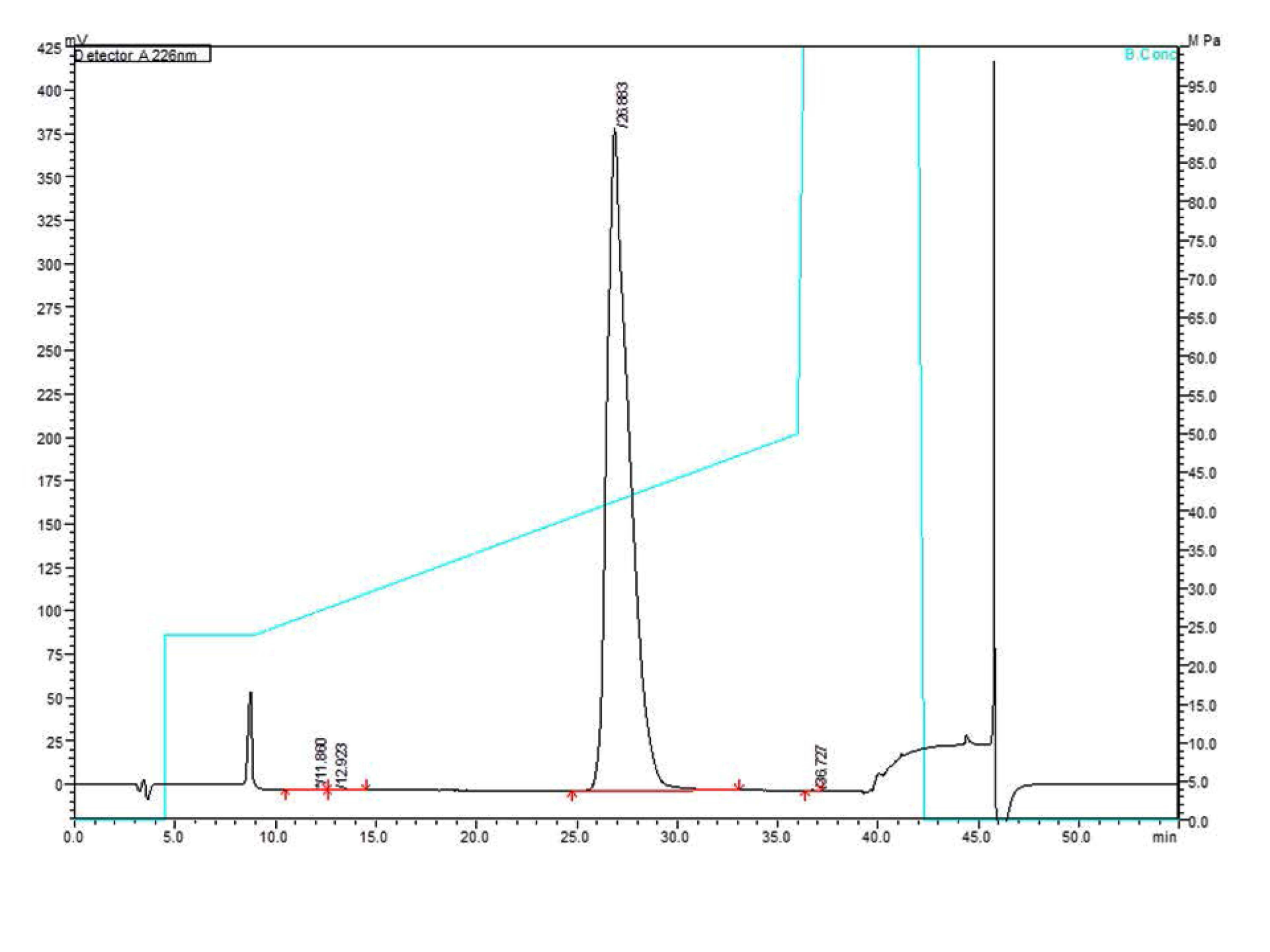
mV
Detector A 226nm
M Pa
B Conc
425
400
375
350
325
300
275
250
225
200
175
150
125
100
75
50
25
0
95.0
90.0
85.0
80.0
75.0
70.0
65.0
60.0
55.0
50.0
45.0
40.0
35.0
30.0
25.0
20.0
15.0
10.0
5.0
0.0
26.883
11.860
12.923
36.727
0.0
5.0
10.0
15.0
20.0
25.0
30.0
35.0
40.0
45.0
50.0
min

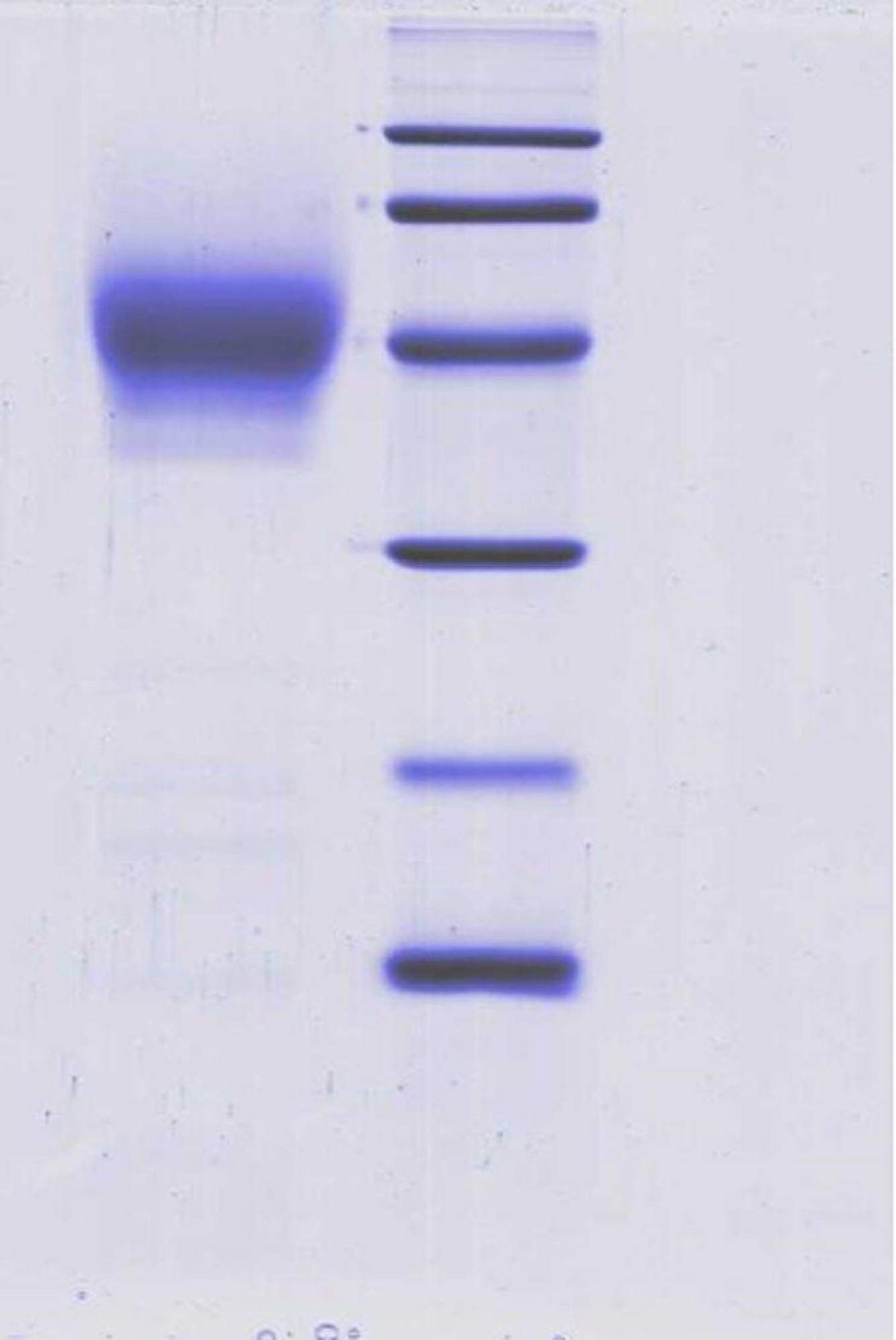
97
66
45
30
20.1
14,4

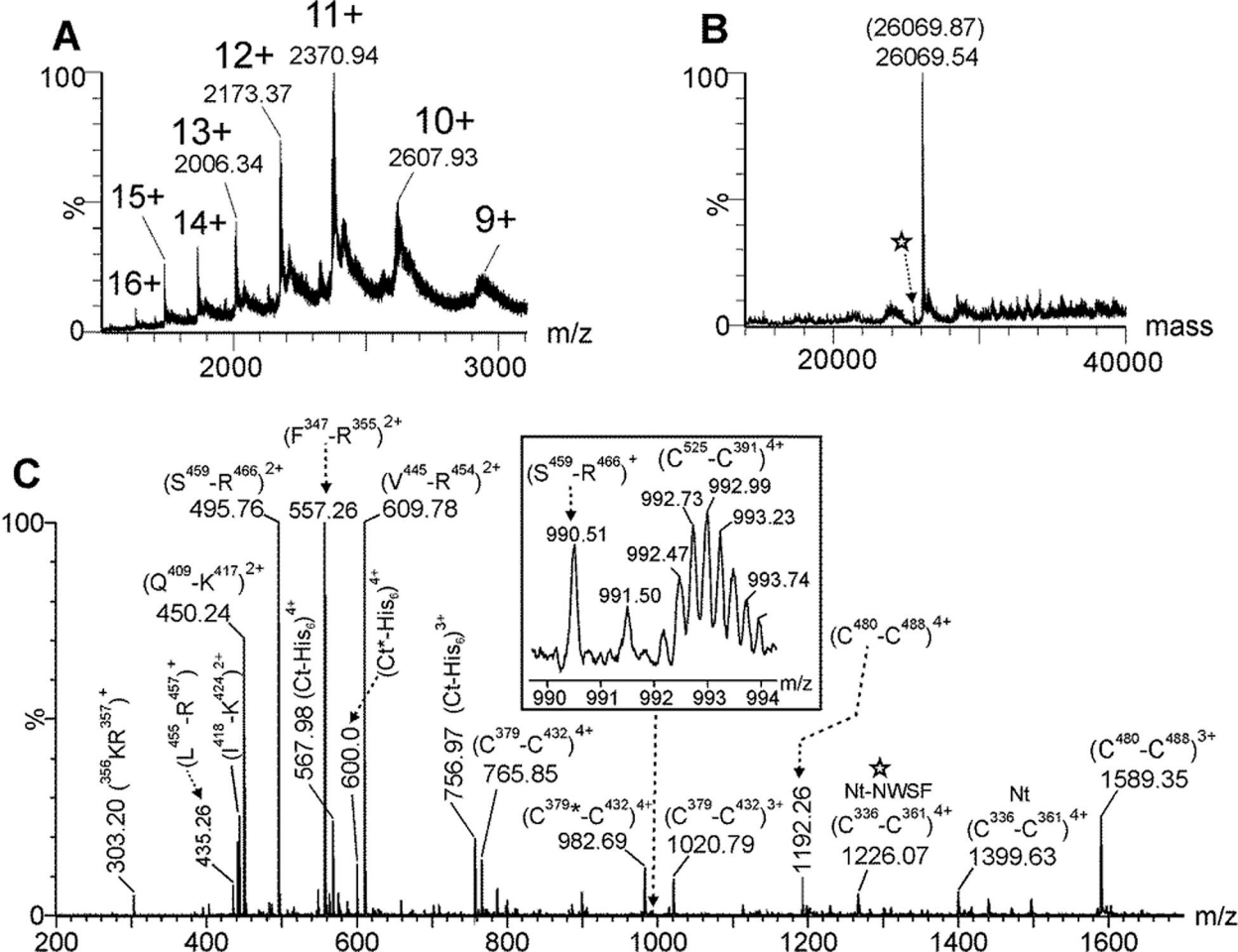
A
11+
12+ 2370.94
2173.37
13+
2006.34
10+
2607.93
15+
14+
9+
16+
100
%
0
2000
3000
m/z
B
(26069.87)
26069.54
100
%
0
20000
40000
mass
C
(F347-R355)2+
(S459-R466)2+
495.76
557.26
(V445-R454)2+
609.78
(Q409-K417)2+
450.24
(Ct-His6)4+
(Ct*-His6)4+
(Ct-His6)3+
(L455-R457)+
(I418-K424)2+
303.20 (356KR357)+
435.26
567.98
600.0
756.97
(C379-C432)4+
765.85
(C379*-C432)4+
982.69
(C379-C432)3+
1020.79
1192.26
(C480-C488)4+
Nt-NWSF
(C336-C361)4+
1226.07
Nt
(C336-C361)4+
1399.63
(C480-C488)3+
1589.35
(S459-R466)+
(C525-C391)4+
992.73
992.99
993.23
990.51
992.47
993.74
991.50
990
991
992
993
994
m/z
100
%
0
200
400
600
800
1000
1200
1400
1600
m/z

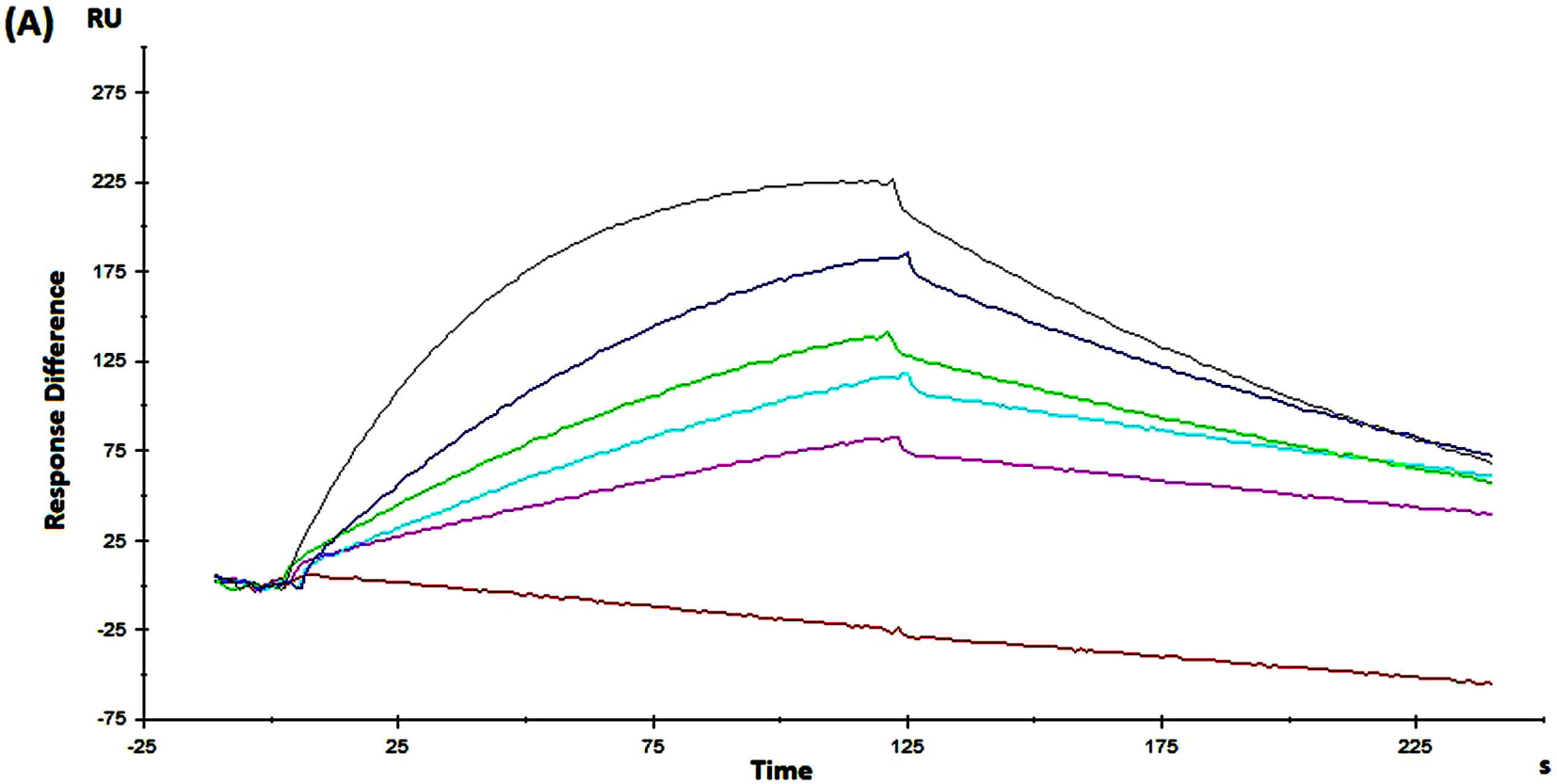
(A)
RU
275
225
175
125
75
25
-25
-75
Response Difference
-25
25
75
125
175
225
Time
s

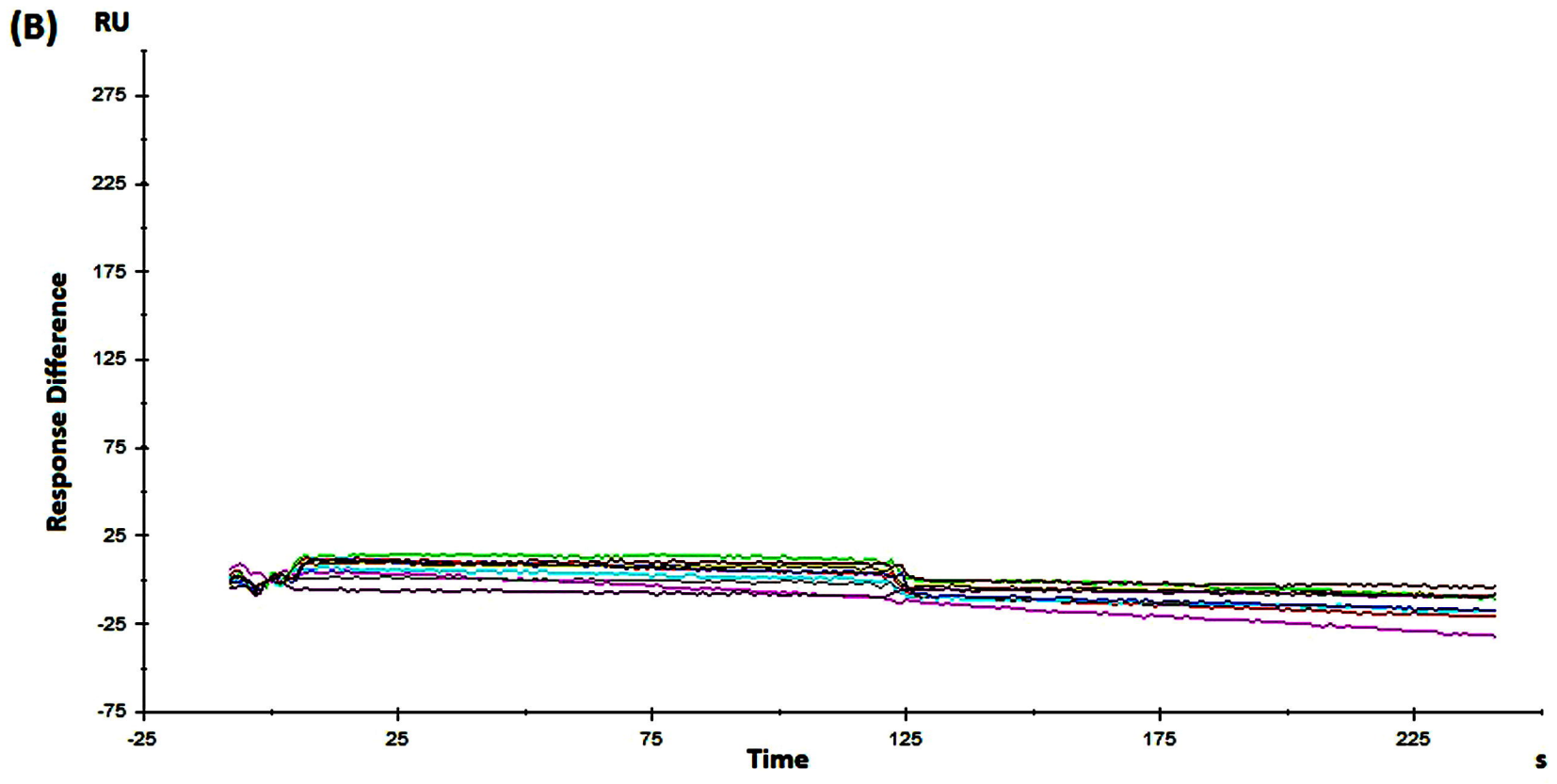
(B)
RU
275
225
175
125
75
25
-25
-75
Response Difference
-25
25
75
125
175
225
Time
s

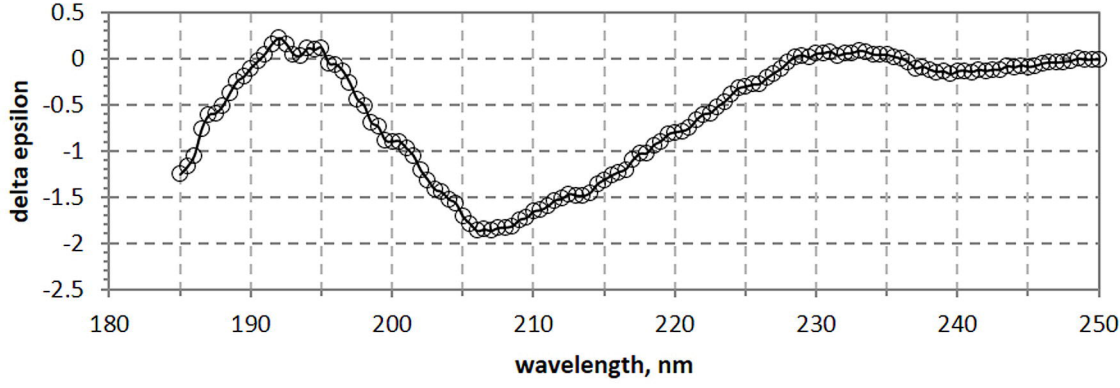
0.5
0
-0.5
-1
-1.5
-2
-2.5
delta epsilon
180
190
200
210
220
230
240
250
wavelength, nm
C-RBD-H6 PP

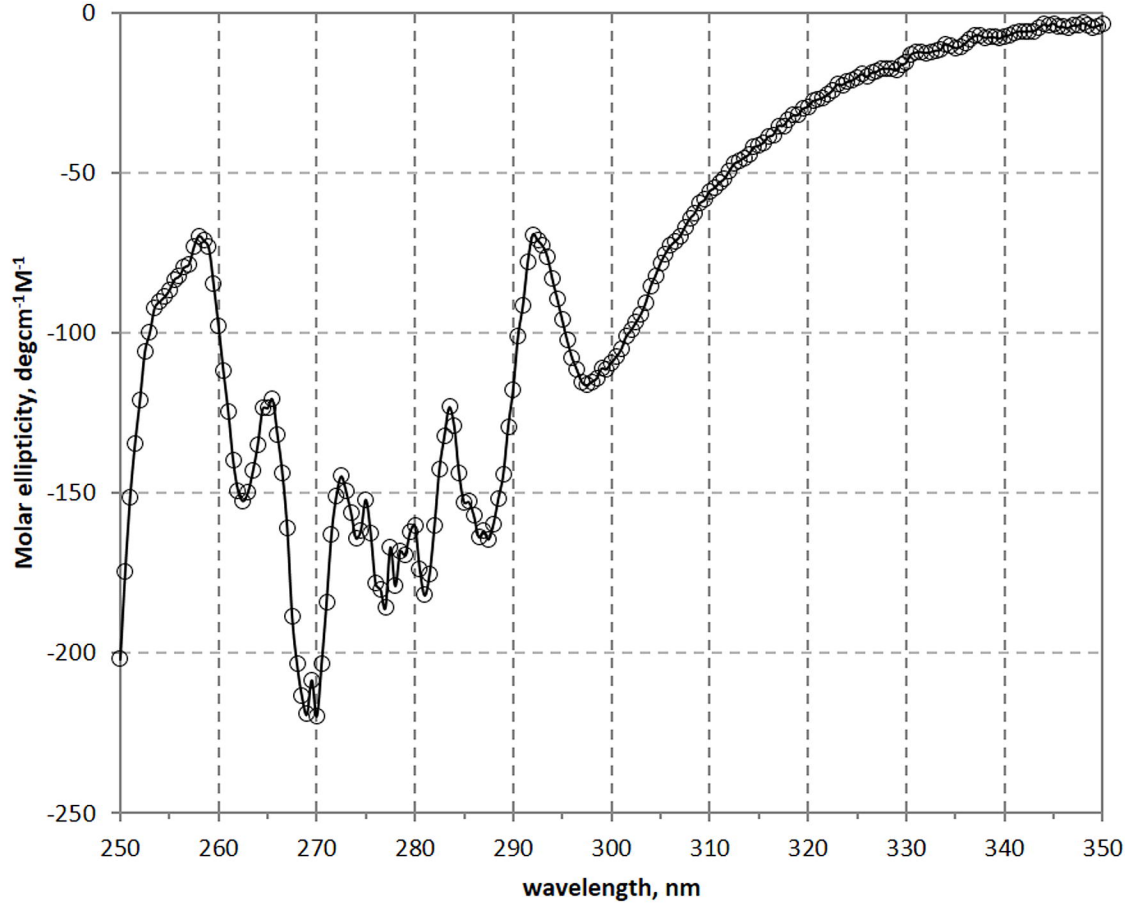
0
-50
-100
-150
-200
-250
Molar ellipticity, degcm-1M-1
250
260
270
280
290
300
310
320
330
340
350
wavelength, nm

C-RBD-H6 PP

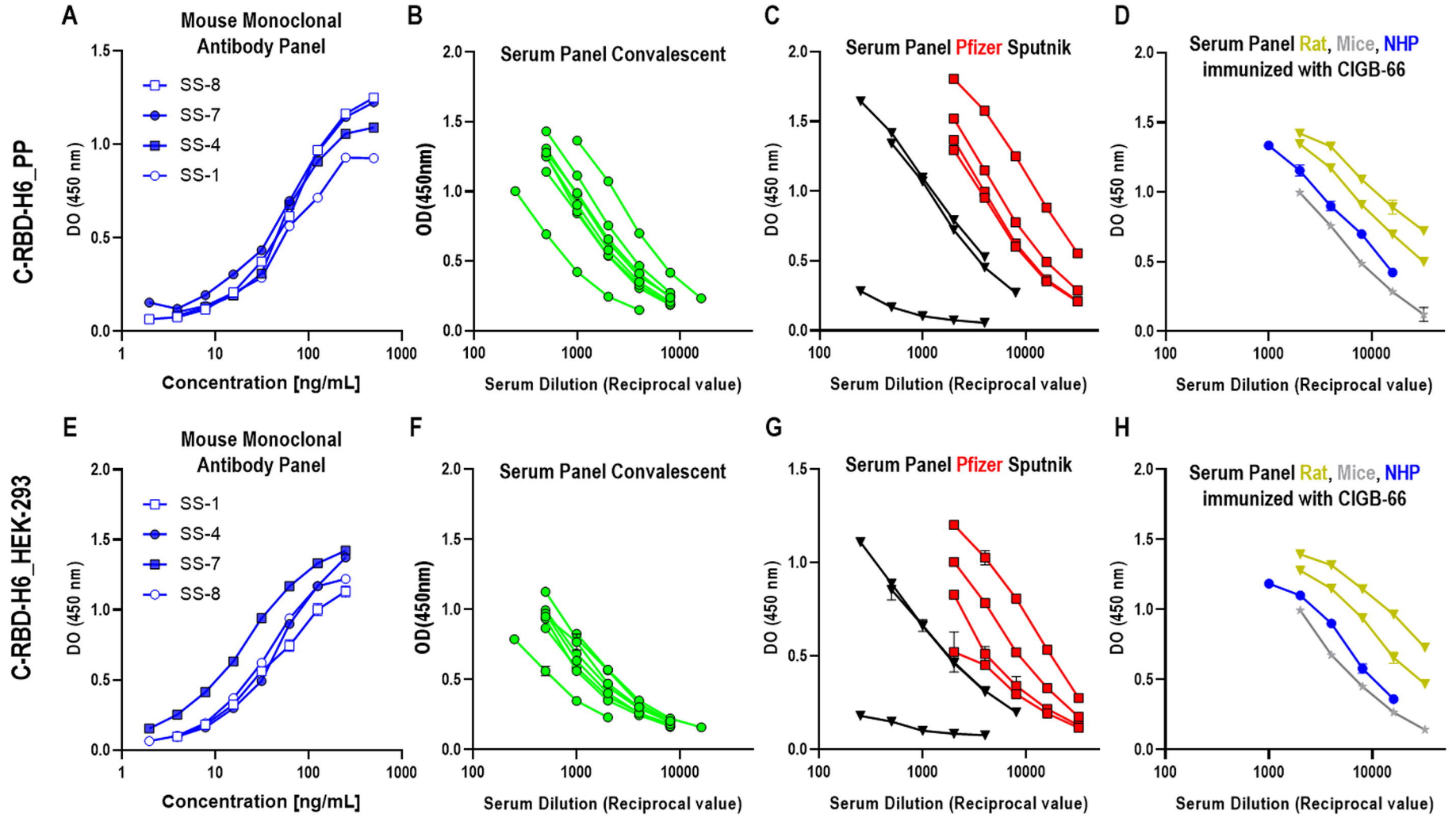
C-RBD-H6_PP
C-RBD-H6_HEK-293
A
Mouse Monoclonal Antibody Panel
SS-8
SS-7
SS-4
SS-1
DO (450 nm)
Concentration [ng/mL]
B
Serum Panel Convalescent
OD(450nm)
Serum Dilution (Reciprocal value)
C
Serum Panel Pfizer Sputnik
D
Serum Panel Rat, Mice, NHP
immunized with CIGB-66
E
F
G
H

I

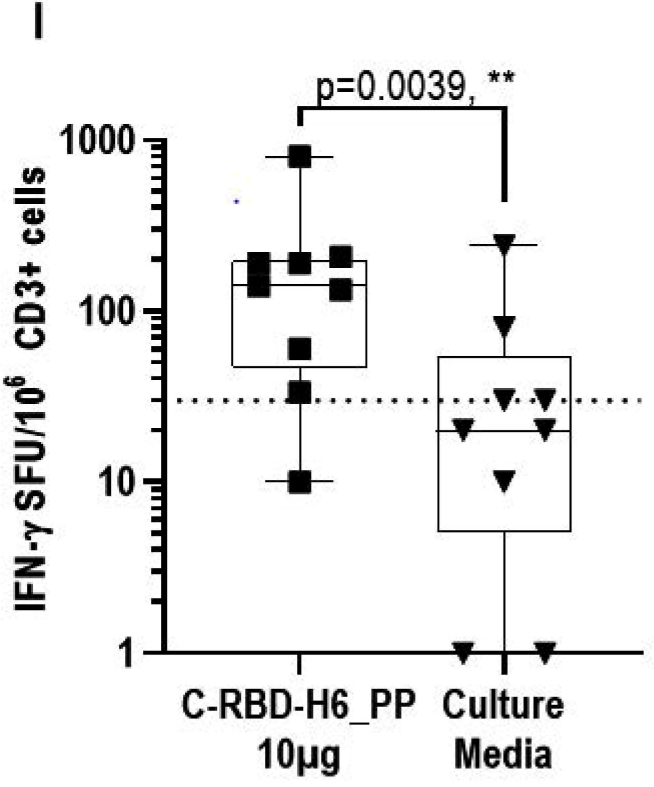
p=0.0039, **
1000
100
10
1
IFN-γ SFU/10^6 CD3+ cells
C-RBD-H6_PP 10µg
Culture Media

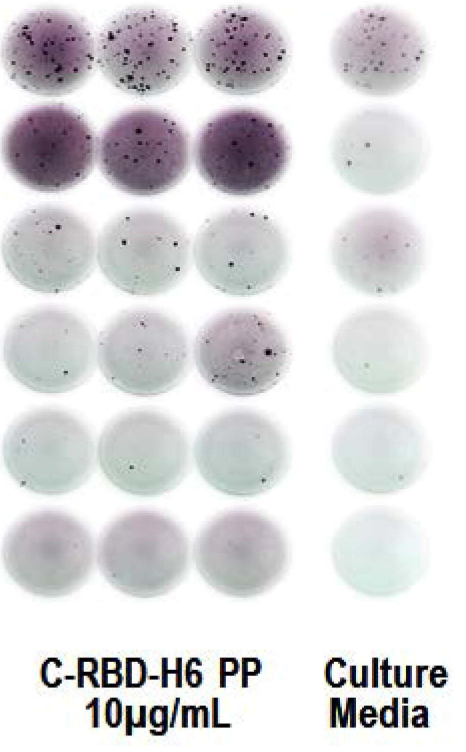
C-RBD-H6 PP 10µg/mL
Culture Media

medRxiv preprint doi: https://doi.org/10.1101/2021.06.29.21259605; this version posted July 3, 2021. The copyright holder for this preprint (which was not certified by peer review) is the author/funder, who has granted medRxiv a license to display the preprint in perpetuity.
It is made available under a CC-BY-NC-ND 4.0 International license .

A

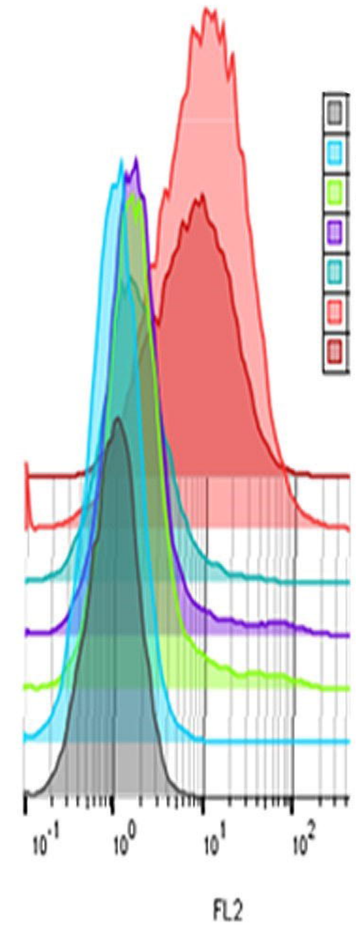

	hFc-RBD Biot	Streptavidin HRP
Neg control Fluorescence	–	+
+ve control hFc-ACE2	+	+
+ve control hFc-RBD 100ug/mL	+	+
L04 C-RBD-H6 PP 100 ug/mL	+	+
L07 C-RBD-H6 PP 100 ug/mL	+	+
+ve control Fluorescence	+	+
Neg control P64K-VEGFH6	+	+

B

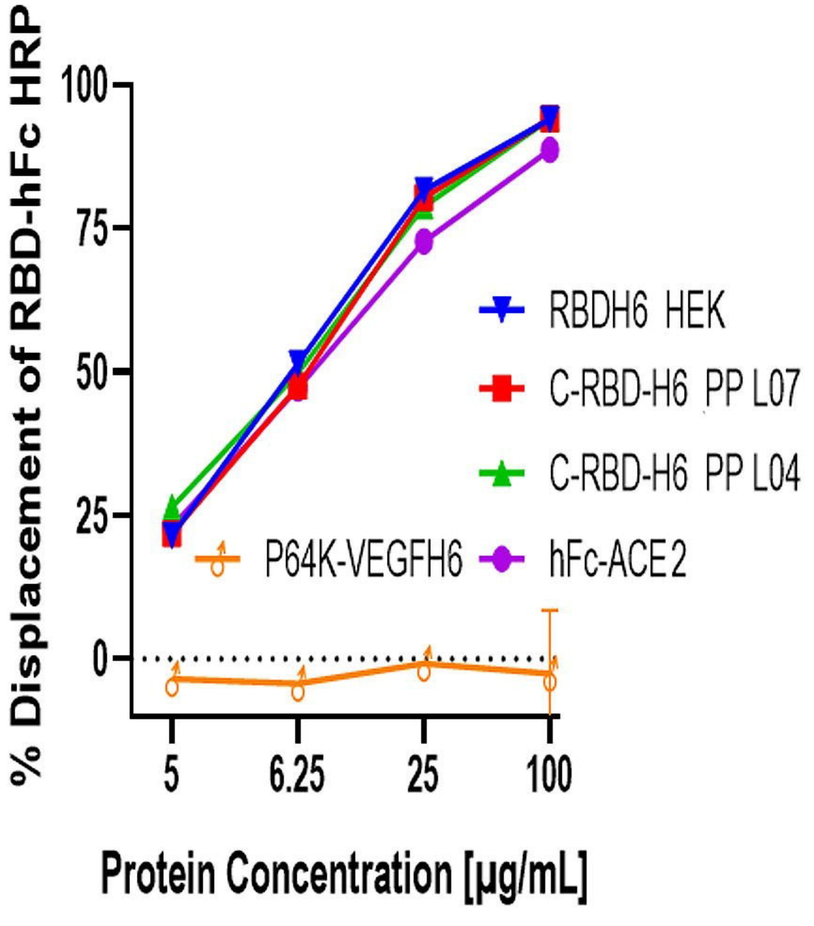

C

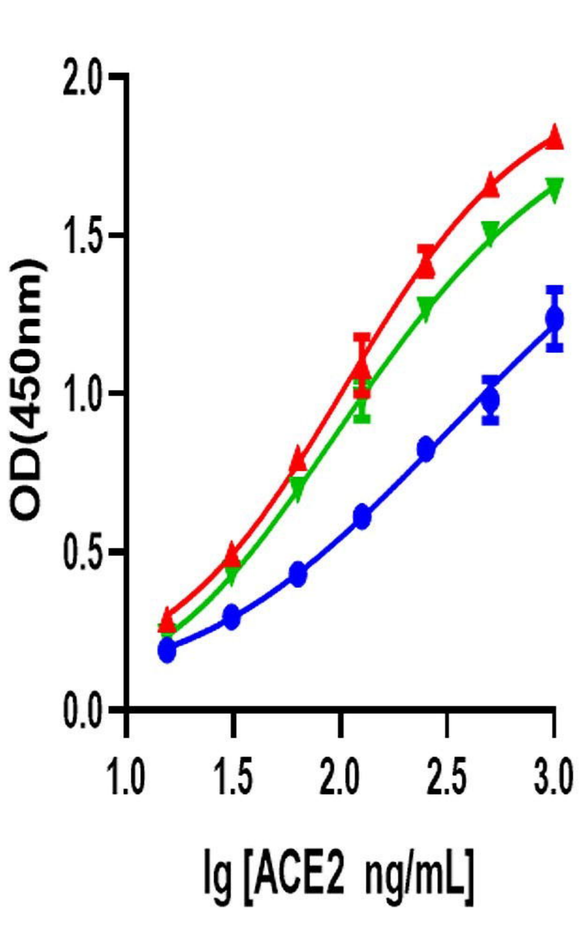

medRxiv preprint doi: https://doi.org/10.1101/2021.06.29.21259605; this version posted July 3, 2021. The copyright holder for this preprint
(which was not certified by peer review) is the author/funder, who has granted medRxiv a license to display the preprint in perpetuity.
It is made available under a CC-BY-NC-ND 4.0 International license .

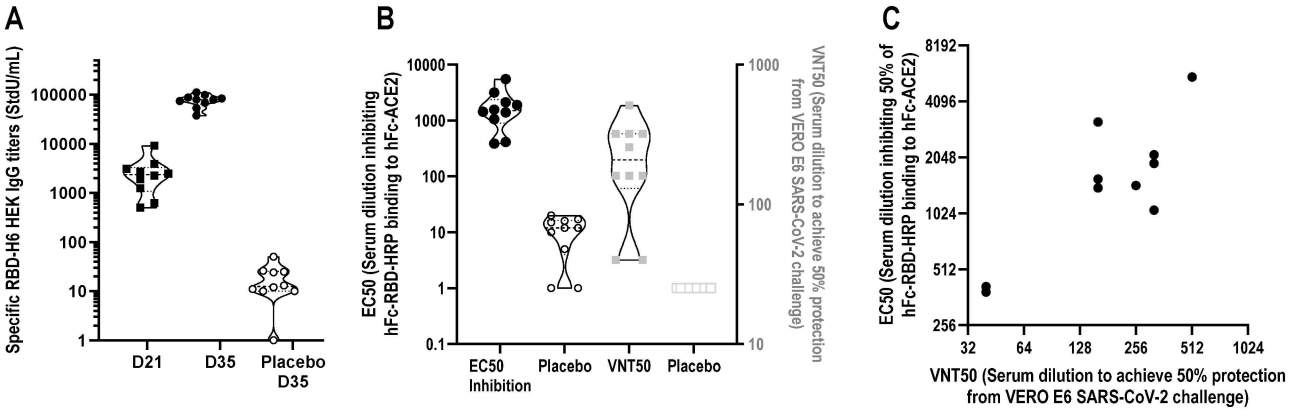

medRxiv preprint doi: https://doi.org/10.1101/2021.06.29.21259605; this version posted July 3, 2021. The copyright holder for this preprint
(which was not certified by peer review) is the author/funder, who has granted medRxiv a license to display the preprint in perpetuity.
It is made available under a CC-BY-NC-ND 4.0 International license .

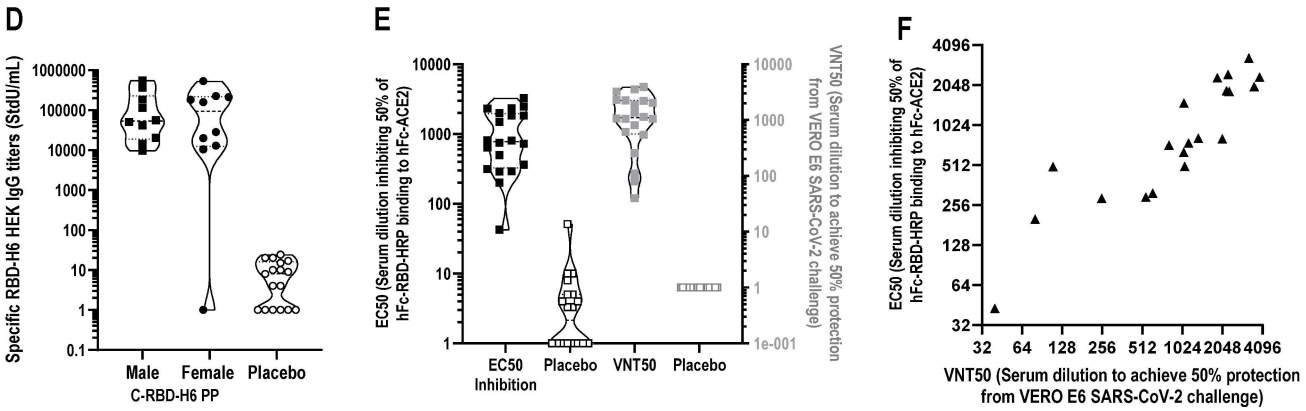

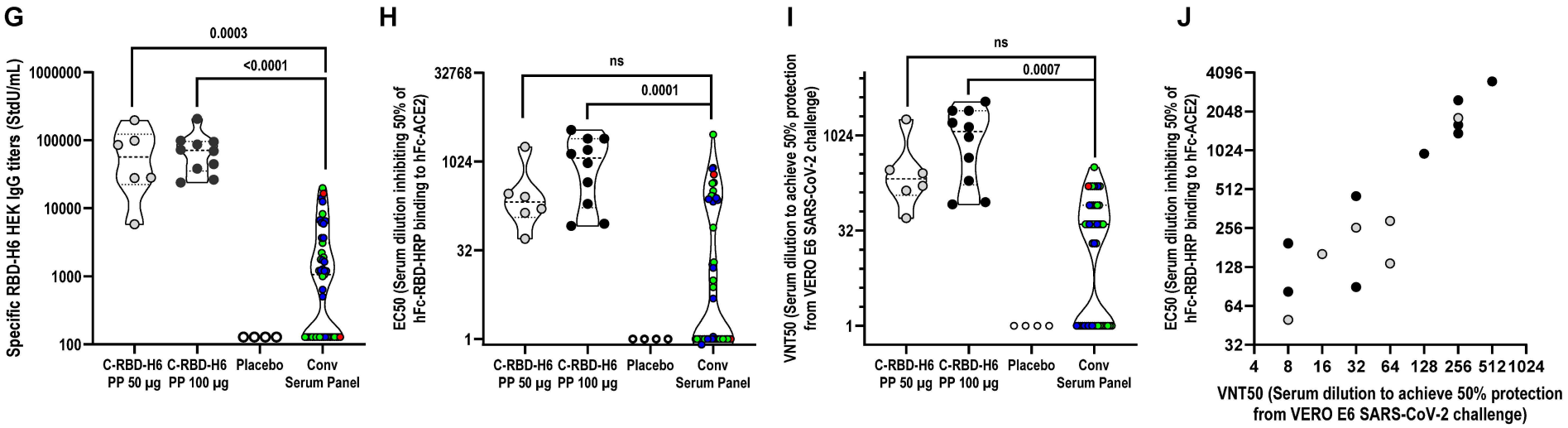
G
0.0003
<0.0001
Specific RBD-H6 HEK IgG titers (StdU/mL)
1000000
100000
10000
1000
100
C-RBD-H6 PP 50 µg
C-RBD-H6 PP 100 µg
Placebo
Conv Serum Panel
H
ns
0.0001
EC50 (Serum dilution inhibiting 50% of hFc-RBD-HRP binding to hFc-ACE2)
32768
1024
32
1
C-RBD-H6 PP 50 µg
C-RBD-H6 PP 100 µg
Placebo
Conv Serum Panel
I
ns
0.0007
VNT50 (Serum dilution to achieve 50% protection from VERO E6 SARS-CoV-2 challenge)
1024
32
1
C-RBD-H6 PP 50 µg
C-RBD-H6 PP 100 µg
Placebo
Conv Serum Panel
J
EC50 (Serum dilution inhibiting 50% of hFc-RBD-HRP binding to hFc-ACE2)
4096
2048
1024
512
256
128
64
32
4
8
16
32
64
128
256
512
1024
VNT50 (Serum dilution to achieve 50% protection from VERO E6 SARS-CoV-2 challenge)
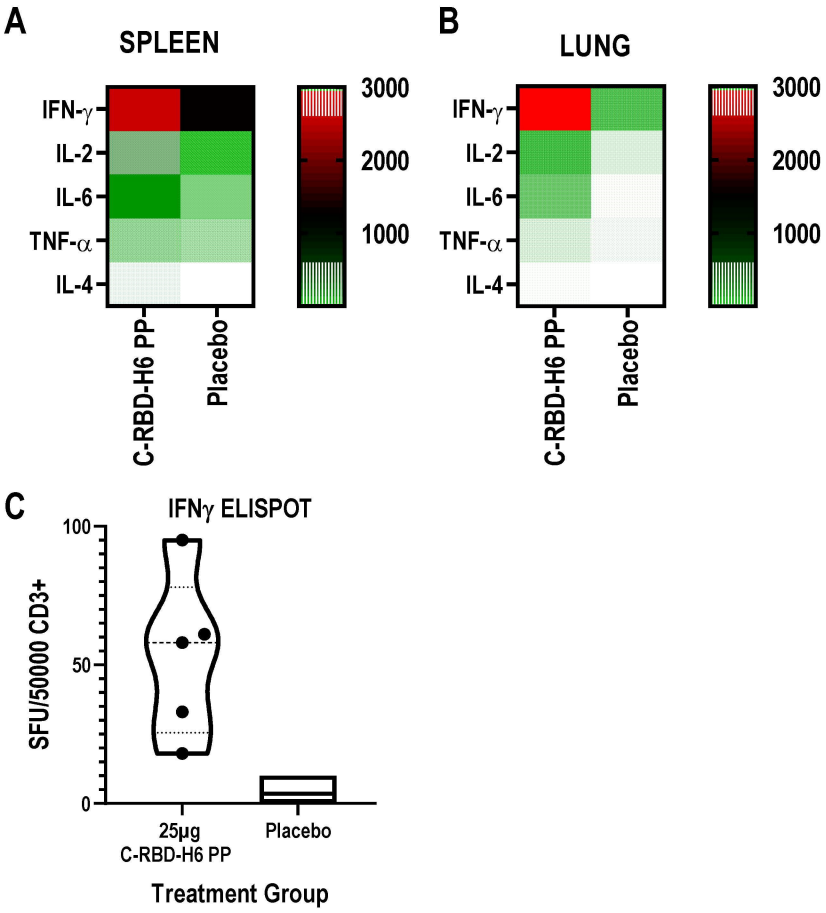
medRxiv preprint doi: https://doi.org/10.1101/2021.06.29.21259605; this version posted July 3, 2021. The copyright holder for this preprint
(which was not certified by peer review) is the author/funder, who has granted medRxiv a license to display the preprint in perpetuity.
It is made available under a CC-BY-NC-ND 4.0 International license .